Citation for published version:
Kumar Nair, PA, Paine, K & Calabria-Holley, J 2023, 'Control of carbonation mechanism in Portland Cement paste using synthetic carbon-capture aluminosilicates', *Journal of CO2 Utilization*.
https://doi.org/10.1016/j.jcou.2023.102391

DOI:
10.1016/j.jcou.2023.102391

Publication date:
2023

Document Version
Publisher's PDF, also known as Version of record

Link to publication

Publisher Rights
CC BY

University of Bath

Alternative formats
If you require this document in an alternative format, please contact:
openaccess@bath.ac.uk

General rights
Copyright and moral rights for the publications made accessible in the public portal are retained by the authors and/or other copyright owners and it is a condition of accessing publications that users recognise and abide by the legal requirements associated with these rights.

Take down policy
If you believe that this document breaches copyright please contact us providing details, and we will remove access to the work immediately and investigate your claim.

Download date: 22. Jan. 2023

Journal of CO2 Utilization 69 (2023) 102391

Contents lists available at ScienceDirect

Journal of CO2 Utilization

journal homepage: www.elsevier.com/locate/jcou

Control of carbonation mechanism in Portland cement paste using synthetic carbon-capture aluminosilicates

Pooja Anil Kumar Nair, Kevin Paine, Juliana Calabria-Holley *

Department of Architecture and Civil Engineering, University of Bath, United Kingdom

ARTICLE INFO

Keywords:
CO_2 curing
Engineered Synthetic aluminosilicates
Nucleation
Water starvation
Pozzolanic reaction
Decalcification

ABSTRACT

In this research, synthetic aluminosilicate nanoparticles in the form of engineered synthetic aluminosilicates (ESA) were added to a cement paste to create a more controlled environment for carbonation and subsequent hydration reactions. To date, early-age CO_2 curing of Portland cement pastes has been shown to reduce the later-age performance due to the decalcification of hydration products and starvation of water by early-age carbonation. However, in this study, it was demonstrated that it is possible to control the carbonation and subsequent hydration reactions through the addition of ESA. Two types of synthetic aluminosilicates were synthesised using organosilanes, tetraethoxysilane (TEOS), and functionalised organosilane, 3-aminopropyltriethoxysilane (APTES). The two aluminosilicates behaved slightly differently, confirming the possibility of altering the carbonation and subsequent hydration reactions. The research demonstrates that tailored nanoparticles enhance carbonate formation by preventing decalcification of the hydration product. The ESA took part in pozzolanic reactions which resulted in no starvation of water on carbonation and led to improved performance at a later age when compared to the samples without ESA. Furthermore, decalcification of portlandite was not observed on the addition of ESA. The carbonation reaction mechanisms on the addition of these ESAs were postulated, and the possibility of increase in carbon uptake without affecting the mechanical performance at later ages were shown.

1. Introduction

Cement is the second most-consumed material after water, and its use is essential to global development. Over 3.5 billion tonnes of cement is produced annually, with approximately 900 kg of CO_2 released for every one tonne of cement produced [1,2]. This accounts for about 5% of the total anthropogenic CO_2 emissions [3–7], The 2030 climate and energy framework by the European Union (EU) has set a target reduction of greenhouse gas (GHG) emission by 40% compared to the levels from 1990 [8]. The emission of CO_2 by burning fossil fuels can be reduced by using alternative fuels like biomass, natural gas, or fuel derived from solid wastes. In the Portland cement production the switch to alternative fuels can reduce CO_2 emissions by 40% [9]. However, a significant contributor to carbon dioxide emission (approximately 60%) comes from the decomposition of carbonates which is a major clinker constituent.

Over the years, several approaches have been taken to reduce the clinker content in cement, through mix design optimisation [4,10–12], and the development of low carbon-cement and binder systems [10–16].

The utilisation of CO_2 within the cement-based matrix [7,17–24] is an innovative approach offering an upcycling solution to reduce the carbon footprint of cement. CO_2 sequestration within the cement matrix has revealed an improvement in performance. This has led to the acceleration of cement hydration kinetics and an increase in strength and durability [19–21,23]. CO_2 capture within the cement binding system is mainly via mixing or curing in a carbonation chamber of freshly hydrating cement. CO_2 utilisation within cement targets the carbonation of anhydrous clinker. Studies on the reaction mechanism of CO_2 with unhydrated clinker phases started in the 1970s [7,20] and it has been observed that the anhydrous calcium silicate phases react with CO_2 in the presence of water to form calcium silicate hydrate gel and calcium carbonate (Eq.1 and Eq. 2) [18]. Monkman et al. [4] suggested three possible reaction mechanisms of fresh cement pastes upon carbonation.

$$3CaO.SiO_2 + (3-x)CO_2 + yH_2O \rightarrow xCaO.SiO_2.yH_2O + (3-x)CaCO_3 \quad (1)$$

$$2CaO.SiO_2 + (2-x)CO_2 + yH_2O \rightarrow xCaO.SiO_2.yH_2O + (2-x)CaCO_3 \quad (2)$$

Furthermore, the hydration products can react with CO_2 in the presence of water to form more calcium carbonate, hydrates of silicates

* Corresponding author.
E-mail address: j.c.holley@bath.ac.uk (J. Calabria-Holley).

https://doi.org/10.1016/j.jcou.2023.102391
Received 29 June 2022; Received in revised form 16 December 2022; Accepted 2 January 2023
Available online 11 January 2023
2212-9820/© 2023 The Authors. Published by Elsevier Ltd. This is an open access article under the CC BY license (http://creativecommons.org/licenses/by/4.0/).

Table 1
Chemical composition of CEM I used (% by mass).

CaO	SiO_2	Al_2O_3	MgO	Fe_2O_3	MgO	Na_2O	Mn_3O_4	BaO	TiO_2	K_2O	LOI
62.8	20.0	5.4	2.2	3.0	2.2	0.1	0.1	0.01	0.2	0.9	3.4

(Eq. 3 and Eq. 4) and aluminates, and water [4,24].

$$CaO.SiO_2.H_2O + CO_2 \rightarrow CaCO_3 + SiO_2 + H_2O \quad (3)$$

$$Ca(OH)_2 + CO_2 \rightarrow CaCO_3 + H_2O \quad (4)$$

The route of carbonation is dependent on several factors like the dissolution rate of the Ca^{2+} [2] and CO_3^{2-}, concentration of CO_2 [21], temperature [25] and relative humidity [19].

The possible stages at which CO_2 can be added to the Portland-cement system are during mixing, batching and curing. Thus, the properties and performance of the hardened cement specimen may be different [24]. The influence of pre-curing and carbonation duration on the strength and microstructure is not fully understood and is still controversial [32]. Zhan et al. [33] found that the compressive strength of CO_2 cured cement paste increased exceptionally in the first two hours. However, currently, the relationship between pre-curing and carbonation curing is not clear. Even though, the reaction mechanisms during early age carbonation are complex and lack conclusive results, this is an upcoming area of interest because of its potential capabilities [4,7,17,18,20–23,26].

Formation of the carbonates in a more tailored environment can offer a certain degree of controllability for hydration and carbonation. Control of the environment is crucial for CO_2 carbonation. For instance, Gerdemann et al. [27] showed that when the particle size of calcium silicate was < 75 μm, temperature 185°C, and pressure 150 bar, the carbonation efficiency was 80%. Ding et al. [28] carbonated calcium silicate of particle size < 20 μm, under different environmental conditions and obtained a carbonation efficiency of 91.1%.

The complexity, lack of clarity, and uncontrollability of the reaction mechanisms during carbonation have led to the consideration that it may be possible to control the reaction mechanisms during carbonation using engineered nanoparticles. For example, research by Santos et al. [29,30] used sol-gel technology to, encapsulate calcium silicate minerals in a porous matrix, enabling efficient carbonation reaction. Sol-gel-based composite particles accelerate the carbonation kinetics enormously [30]. For instance, calcium silicate (wollastonite) containing 17% more CaO than sol-gel modified wollastonite (SAW40) showed only 51.16% calcite formation, whereas SAW40 showed 81% calcite formation according to the Rietveld method. The engineered composite particles created an encapsulation that prevented agglomeration of powder which in the case of cement would be the anhydrous clinker and thus increased the surface area of the reaction [30]. The sol-gel-based CO_2 capture technique inhibited the formation of the passivation layer (formation of carbonates and hydration product) over the anhydrous clinkwhich could reduce the carbonate formation efficiency. The possibilities for sol-gel technology to embed cementitious materials into a silica matrix can also increase the carbonation efficiency due to the availability of higher surface area.

Given the above considerations, this research investigated ways to enhance the carbonation mechanism within the Portland cement matrix using engineered synthetic aluminosilicates (ESA). This research also established the reaction mechanisms and subsequent carbonate and hydrate formation on the addition of these ESA. A detailed investigation of the evolution of the chemical and microstructural changes on cement pastes under coupled CO_2-water curing environment was carried out. Furthermore, investigations on the possibilities for preventing water starvation and interruption of subsequent reaction mechanisms were carried out. The CO_2 utilisation within the cement paste using a combined curing system was examined at a microstructural level using x-ray powder diffraction (XRD), thermogravimetric analysis (TGA), and nitrogen adsorption and mercury intrusion porosimetry (MIP).

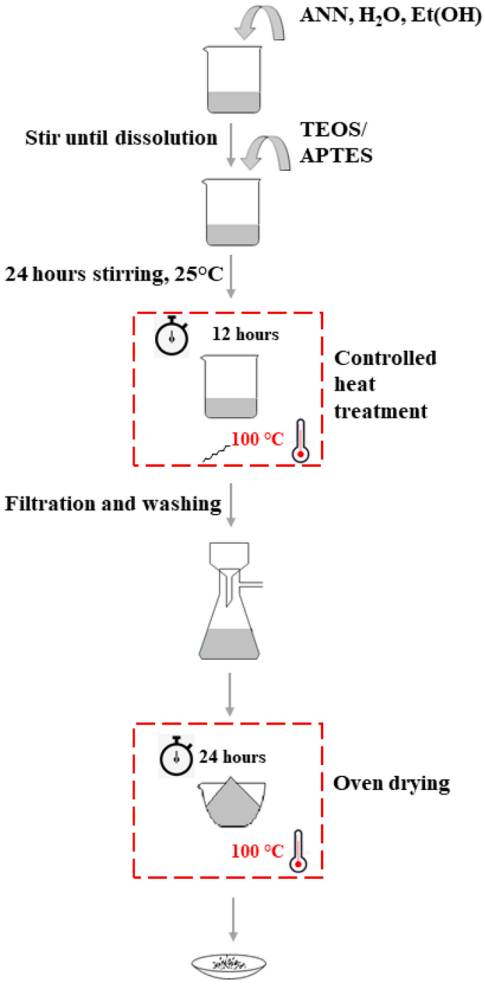

Fig. 1. Schematic representation of synthesis of sol-gel aluminosilicates.

2. Experimental methods and materials

In this research, ESA were added to cement pastes to study the controllability and alterations in chemical and microstructure on early-age carbonation. Cement paste samples were cast for microstructural analysis and cement mortar samples were cast for physical performance test (compressive strength test). To facilitate CO_2 diffusion into the pores of the cement paste, the samples were pre-cured for two hours in an environmental chamber after 24 hours of in-mould curing.

2.1. Materials

The cement used was Dragon Alfa CEM I 42.5 R, conforming to BS EN 197–1. The oxide composition of the cement, as determined by X-ray fluorescence (XRF) spectroscopy, is given in Table 1. For the sol-gel syntheses, the silica precursors used were tetraethoxysilane (TEOS) and 3-aminopropyltriethoxysilane (APTES), both supplied by Fisher Scientific. The alumina precursor was aluminium nitrate nonahydrate

Table 2
Physical properties of the materials.

Designation	Silica donor ()	Density (g/cm^3)	Specific surface area (m^2/g)
ESA-TEOS	-O-Si-OC_2H_5	2.02	646.88
ESA-APTES	-O-Si-C_3H_6-NH_2	1.45	-

Table 3
Mix design for cement paste.

Sample Id	Cement (g)	ESA		Water (g)	w/ (c+a)
		Mass (g)	ESA content (% by mass of PC)		
CTRL	350	-	-	140	0.4
TBA	346.5	3.5	1	140	0.4
ABA	346.5	3.5	1	140	0.4

Table 4
Mix design for cement mortar.

Sample Id	Cement (g)	ESA		Standard sand (g)	Water (g)	w/ (c+a)
		Mass (g)	ESA content (% by mass of PC)			
CTRL	4050	-	-	12150	1620	0.4
TBA	4009.5	40.5	1	12150	1620	0.4
ABA	4009.5	40.5	1	12150	1620	0.4

(ANN) supplied by VWR chemicals. Ethanol was supplied by Fisher Scientific.

2.2. Synthesis of sol-gel aluminosilicates

ESA were synthesised using sol-gel technology to improve the controllability of the carbonation mechanism and enhance the CO_2 fixation at all ages. The synthesis procedure, material properties and the CO_2 capture capacity of the ESA are described in detail elsewhere [31]. To investigate the ability of sol-gel technology in controlling the carbonation mechanism, two types of aluminosilicates were used. The alumina source, ANN was the same for both the types of aluminosilicates, however, the silica precursor was varied. The first aluminosilicate used an organosilane precursor, TEOS. Whereas, for the second aluminosilicate, a functionalised organosilane, APTES, was used. The solvent used in both cases was ethanol. The syntheses were carried out with distilled water. Initially, ethanol and water were mixed with ANN until its complete dissolution. Following this, TEOS or APTES was added to produce aluminosilicate or amine-aluminosilicate synthesis, respectively. The mixes were synthesised for 24 hours, after which they were heat-treated to 100 ℃ in a controlled environment with a dwell time of 12 hours and a two-hour dwell time every 20 ℃. The rate of increase in temperature was 0.5 ℃/minute. Following this, the samples were washed with water and then dried at 100 ℃. The molar ratio used was $1SiO_2$:10 H_2O:10Et(OH):$0.05Al_2O_3$. Fig. 1 shows a schematic representation of the synthesis of the aluminosilicate. The aluminosilicates contained 5% of alumina. The physical properties of the materials are given in Table 2.

2.3. Cement sample preparation

Cement pastes were made at a water to solids (cement + ESA), w/(c + ESA) ratio of 0.4 and cast in 40 mm cube moulds. The ESA replaced 1% by mass of cement. The mix design for paste and mortar samples are given in Table 3 and Table 4 respectively. Firstly, the ESA were dispersed in the mix water and added to the cement. The samples were prepared to conform with the EN 196–1. Fig. 2 shows the schematic representation of the curing procedure comprising three stages. The Stage I (Pre-conditioning) consisted of in mould curing and environmental chamber curing. Environmental chamber curing was crucial to remove excess water in the initially hydrated in-mould cured sample, to facilitate CO_2 diffusion during stage II (CO_2 curing). Following stage II, the samples underwent post curing. Post curing (stage III) allowed further hydration of the unreacted hydraulic phases. Fig. 3 shows the schematic representation of systematic curing procedure for samples investigated in this research. All samples were in mould cured in plastic bags at 20 for 24 hours immediately after casting (stage I). The samples were then demoulded and separated into two sets. One set was water cured until the age of testing (water curing only, see Fig. 3) and the other set of samples were cured in environmental chamber for 2 hours at 20 and 50% RH. The only water cured sample (former set) was to study the hydration mechanism of ESA in cement. The environmental chamber cured samples from Stage I (latter set) were further divided into two sets, one set was CO_2 cured (stage II) for 2 and 24 hours at 20 and ≈ 50% RH and the other was water cured until the age of testing (non-carbonated route, see Fig. 3) Following the curing procedure, as shown in Table 5 and Fig. 3, the samples were water cured at 20 ℃ until the age of testing. The age accounted for the samples commenced immediately after casting. The sample designation was based on its curing protocol ('E' for environmental chamber curing followed by 'C' for CO_2 curing) followed by the sample Id as the prefix (Table 4). The prefix Id for samples without aluminosilicates was CTRL; samples with TEOS and APTES based aluminosilicates as the additive was designated as 'TBA' and 'ABA' respectively. The samples were also weighed at the end of pre-curing

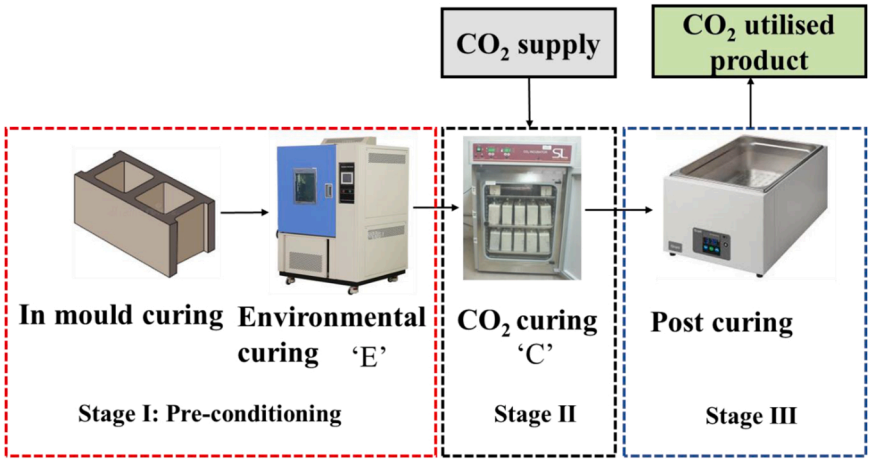

Fig. 2. Schematic representation of curing stages. Note: Not all samples went through Environmental chamber curing (E) in Stage I and CO_2 curing in Stage II (C).

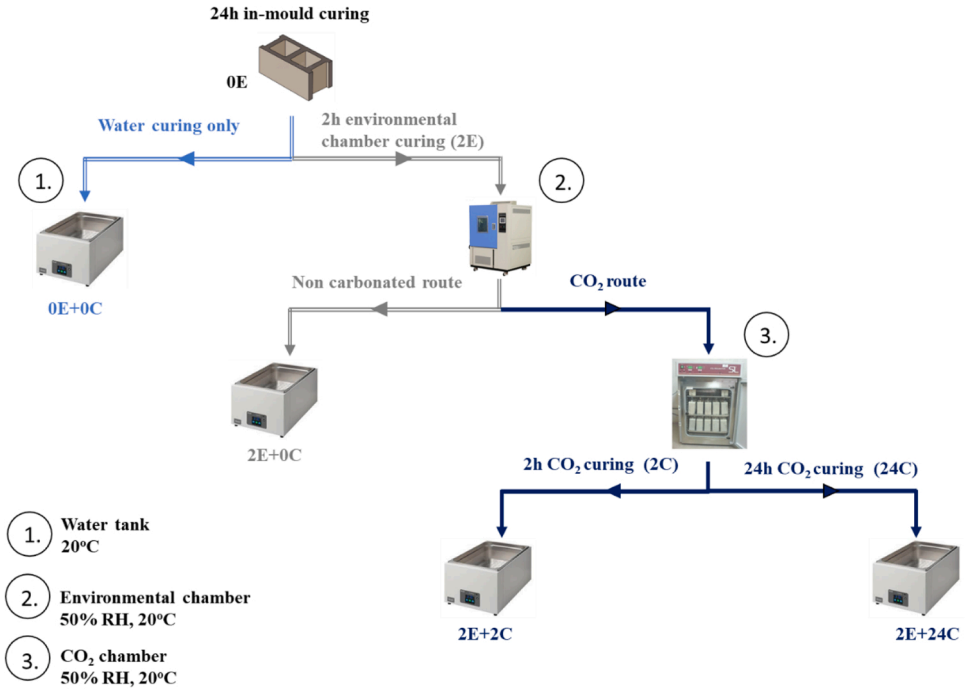

Fig. 3. Schematic representation of sample curing.

Table 5
Curing protocol for each sample (see Fig. 3 to follow the curing procedure of samples).

Sample designation	In mould curing (hours)	Environmental chamber curing			CO_2 curing	
		RH (%)	Duration (hours)	Temperature (℃)	Duration (hours)	Temperature (℃)
CTRL-0E+ 0C	24	50	0	0	0	20
CTRL-2E+ 0C	24	50	2	20	0	20
CTRL-2E+ 2C	24	50	2	20	2	20
CTRL-2E+ 24C	24	50	2	20	24	20
TBA-0E+ 0C	24	50	0	0	0	20
TBA-2E+ 0C	24	50	2	20	0	20
TBA-2E+ 2C	24	50	2	20	2	20
TBA-2E+ 24C	24	50	2	20	24	20
ABA-0E+ 0C	24	50	0	0	0	20
ABA-2E+ 0C	24	50	2	20	0	20
ABA-2E+ 2C	24	50	2	20	2	20
ABA-2E+ 24C	24	50	2	20	24	20

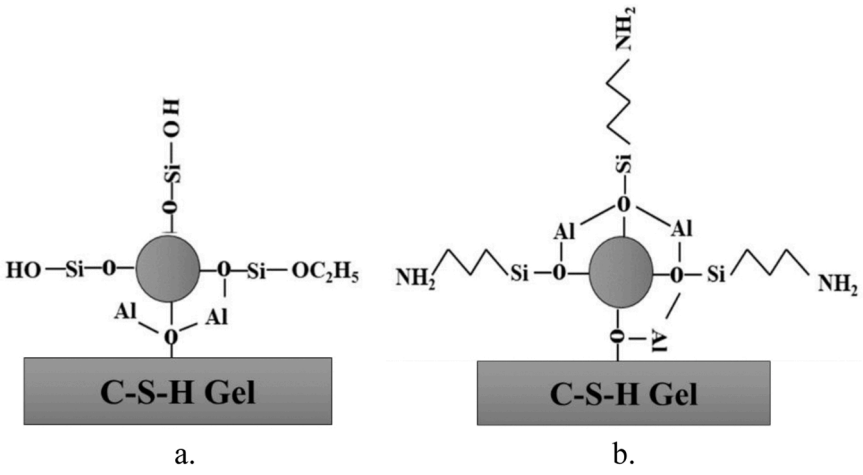

Fig. 4. Synthetic aluminosilicate modified cement pastes; a. ESA-TEOS; b. ESA-APTES.

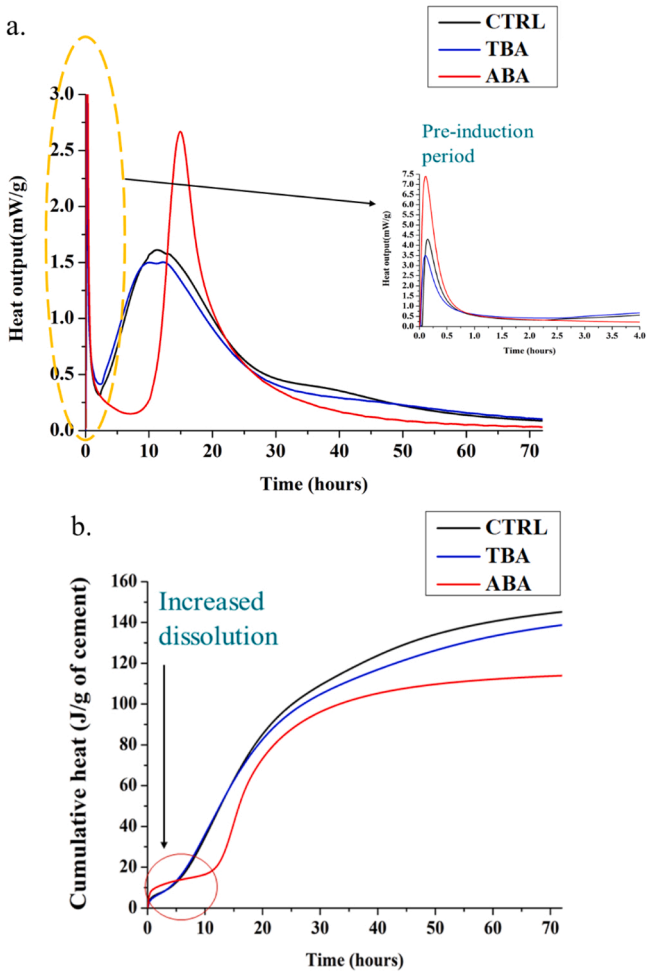

Fig. 5. Influence of the aluminosilicates on the heat of evolution during cement hydration; a. heat flow and b. cumulative heat output.

and CO_2 curing to determine the water loss. The water loss during the CO_2 curing was determined by deducting the mass of CO_2 from the total mass variation [26]. Fig. 4.

The curing conditions for the samples were set in accordance with the environmental conditions that gave the best-suited environment for enhanced CO_2 uptake during CO_2 curing [26].

Fig. 4 shows how the synthesised ESA interact with the silicate phases in the cement pastes. The ESA-TEOS consisted of hydrolysable alkoxy groups (-OC_2H_5). The ESA-APTES with unhydrolysable -CH_2CHNH_2 groups have the ability to create a homogeneously dispersed reaction medium due to the presence of hydrophilic NH_2 ending group [32].

2.4. Characterisation methods

The hydration kinetics of the ESA added cement pastes were investigated for a duration of 72 hours at 20ºC using isothermal conduction calorimetry (Calmetrix I-Cal 4000). Microstructural characterisation was conducted for all samples at 3, 7 and 28 days. All the fractured samples at the three ages underwent arresting of hydration according to technique described elsewhere [33]. For chemical analysis techniques (TGA and XRD), the ground samples were oven dried at 60. For microstructural evolution and morphological changes (Nitrogen (N_2) adsorption, MIP), the method used to arrest hydration was solvent exchange [32].

The crystalline phases of the carbonated and hydrated samples were analysed using WinXPOW PKS_2.01 Version. A X-ray diffractometer

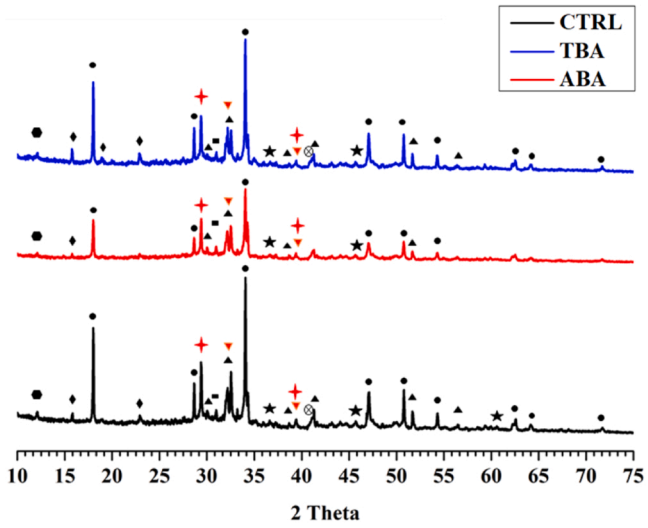

Fig. 6. X-ray diffraction pattern of 3-days hydrated samples.

with Cu-Kα radiation of step size 0.015º/sec and a scan interval of 2–75º 2θ was used for XRD. A thermal analyser (NETZSCH STA 449F1 Jupiter) was used for TGA, for which approximately 30 mg of the powdered sample were placed in an alumina crucible with a test ramp of 20 ℃/min over a range of 30–950 ℃ with nitrogen as the carrier gas.

The pore structure of cured samples in water and CO_2 were assessed by joint N_2 adsorption and MIP. N_2 adsorption was performed at 77 K using a 3 Flex Micromeritics after degassing at 60 for 12 hours with a ramp of 10/minute. For the MIP testing, a contact angle of 140° and surface tension of 0.48 N/m was used. The pressure was applied in two stages on the same sample. At first the sample was tested on Thermo Scientific Pascal 140 Series where a pressure of up to 140 kPa was applied using air and then the sample was further tested on a Thermo Scientific Pascal 440 Series where pressure up to 400 MPa was applied using a piston by pumping oil.

Compression strength test was carried out on the prepared 28 days ages mortar samples in accordance with BS EN 196–1. The prisms were tested for flexure following which the broken halves were tested for compression. The compressive strength results were the arithmetic mean from the set of five broken halves of the flexure test results. In cases of the strength results falling outside the ± 10% of the mean value were discarded and the mean of strength results of the remaining five samples were recalculated.

3. Results

3.1. Hydration mechanism on the addition of synthetic aluminosilicates before carbonation curing

3.1.1. Hydration rate

Fig. 5a and b show the heat evolution and cumulative heat of the TBA and ABA, respectively. The overall trend of the profile remains similar, which indicates that the general reaction of dissolution of ions in the pore solution and precipitation remained the same. However, there was a shift in the dormant stage and variation in the intensity of the heat profile for ABA (Fig. 5a). The pre-induction stage is highlighted (Fig. 5a) as its plays an important role in the early age hydration mechanics. This is because this stage is affected by the rate of cement dissolution, nucleation, precipitation, and subsequent hydration product formation. Initial dissolution for ABA lasted for about an hour, followed by an extended dormant stage for 6 hours when compared to the other samples, which is consistent with the literature [32,34]. The increase in the dissolution activity was also seen in the cumulative heat result (Fig. 5b). On the other hand, it was seen that the TBA followed similar kinetics as

Table 6
Key for XRD.

✦	$CaCO_3$
●	Portlandite
▲	C_3S
▼	C_2S
♦	AFt
■	Monocarboaluminate
★	Hemicarboaluminate
⊗	C_3A
⬢	Ferrite

that of the neat cement paste (CTRL). This trend is similar to the contribution of the total energy released by CTRL over the initial 24 hours.

3.1.2. Phase analysis

The XRD pattern of the 3 days aged sample is presented in Fig. 6. Table 6 shows the key for the identified phases of the samples. In general, the trend of peaks among all the three samples were similar, although the intensity of the peaks differed. This indicated that further quantitative results were required to determine the amount of remaining anhydrous clinker and products formed. Hence as described earlier, quantitative TGA was conducted to further investigate the reaction mechanisms (Fig. 7).

The results were calculated from the DTG curves. The portlandite and calcium carbonate were calculated between the temperature range 420–540C and 550–945C, respectively, using the tangent method. The total bound water was calculated using a stepwise method between the temperature range 60–540C and subtracted from the portlandite content. In general, both ESA-TEOS and ESA-APTES altered the cement paste in terms of the hydration products formed. At 24 hours, there was the same amount of bound water for all the samples, however, the portlandite content differed (Fig. 7).

Furthermore, ABA had the least portlandite followed by TBA. At 3 days, the bound water and the portlandite contents were highest for TBA. The decrease in portlandite is seen for CTRL due to the atmospheric carbonation on handling. Fig. 8 represents the bound water, portlandite and calcium carbonate contents, respectively, for both control and the samples modified with the synthetic aluminosilicates at 1, 7 and 28 days. On ageing, the ABA showed an increase in bound water with a decrease in portlandite compared to the control, suggesting a pozzolanic reaction. In general, ABA has shown a rise in carbonates compared to CTRL and TBA. The carbonates (%) drop sharply from 7 days to 28 days for ABA. This could be because the reverse of Eq.3 could have happened as the bound water increased sharply from 7 days to 28 days. However, this requires further investigation. On closer observation at 7 days, even though, the bound water for aluminosilicate modified samples were the same, the variation in the portlandite content indicated that the

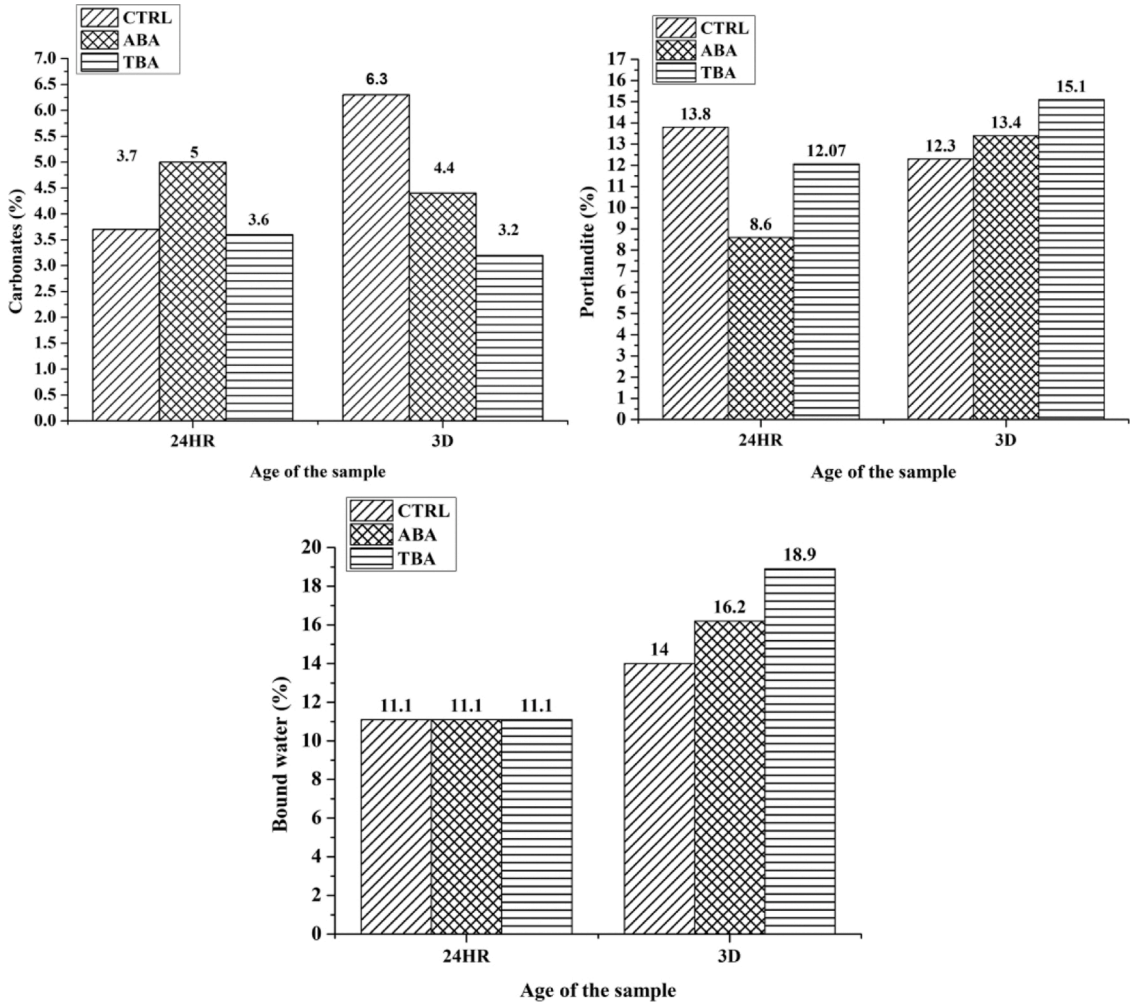

Fig. 7. Investigation of 3-day hydration mechanism using thermogravimetric analysis.

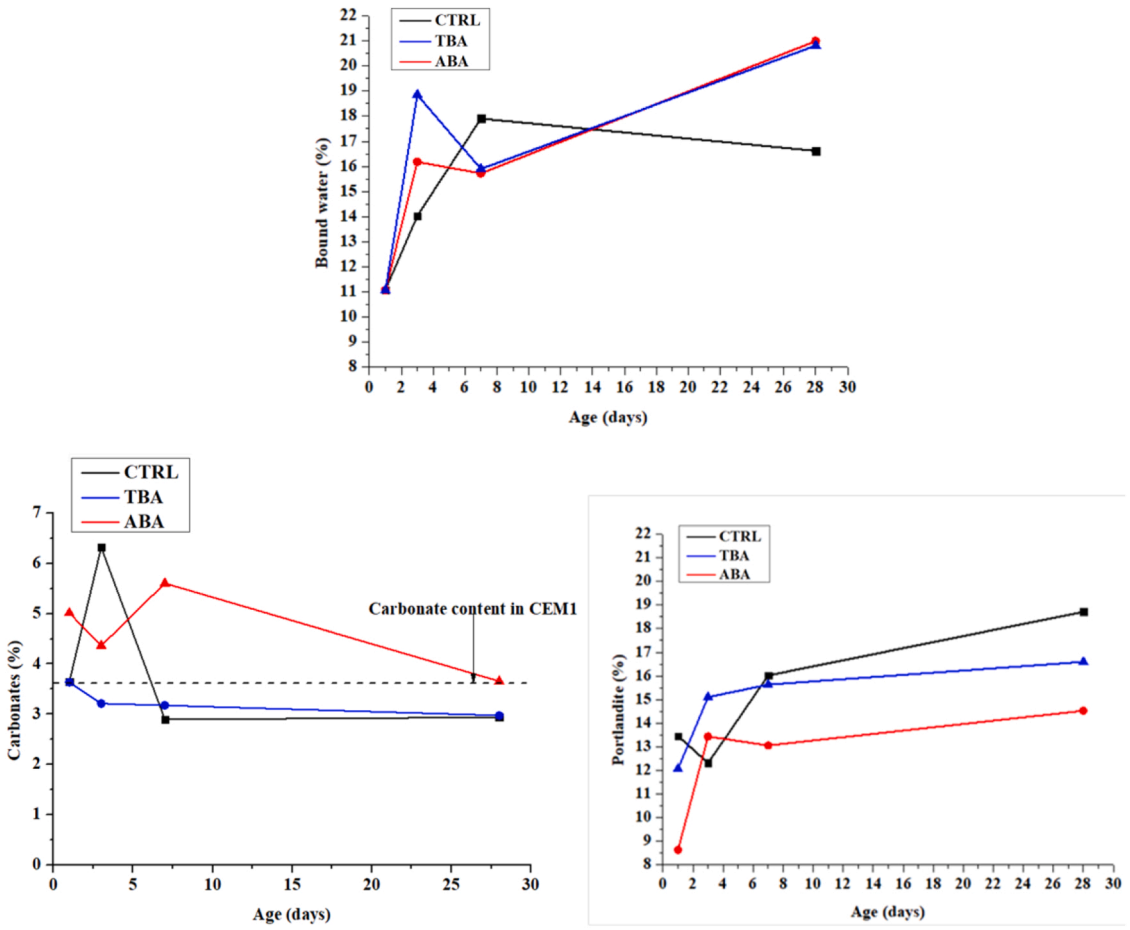

Fig. 8. Thermogravimetric analysis to study the hydration mechanism of non-carbonated TBA and ABA at 3, 7 and 28 days.

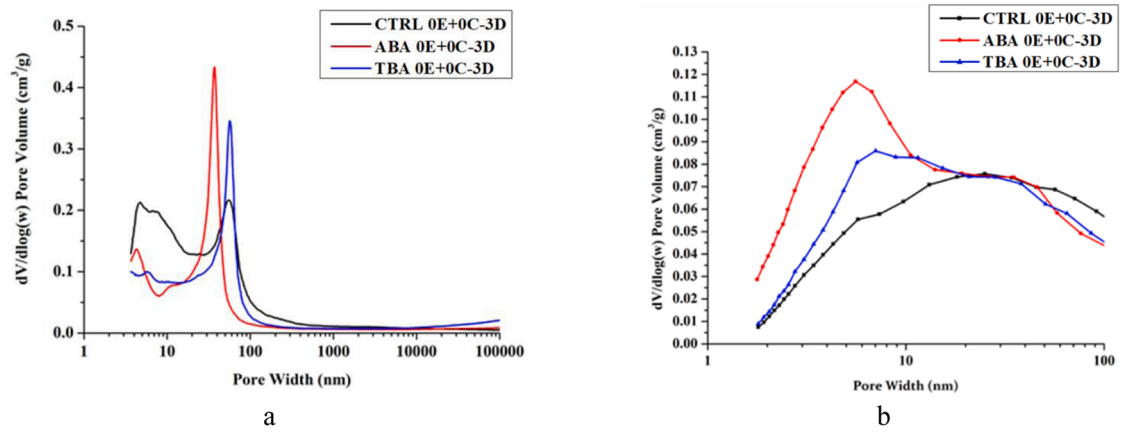

Fig. 9. Pore volume distribution of 3-day TBA and ABA samples to investigate changes in pore structure; a. MIP; b. N_2 adsorption.

Table 7
Pore size ranges and highest peak position for the 3-day aged samples.

	N_2 adsorption (nm)		MIP (nm)			
			Mode 1		Mode 2	
	Peak range	Highest peak	Peak range	Highest peak	Peak range	Highest peak
CTRL	1.8–91.7	25.0	3.7–16.1	4.8	35.1–77.4	55.5
ABA	1.8–91.7	5.8	-	-	22.7–62.2	36.7
TBA	1.8–91.7	7.4	-	-	36.2–73.7	56.5

hydration reaction mechanism of each of the synthetic aluminosilicate were different.

3.1.3. *Pore structure analysis*

The pore structure was investigated at two different scales: meso-macropores between 2 and 70 nm and capillary pores $\geq$ 70 nm. Fig. 8 shows the pore size distribution of 3 days aged samples using nitrogen adsorption and MIP. The results of MIP for the ESA-TEOS and ESA-APTES containing samples show a pore size range from 10 to 100 nm but no pores were observed below 10 nm (Fig. 9a). This could be because the pore sizes of ABA and TBA were smaller than the minimum

Table 8
Pore structure characteristics using Nitrogen adsorption and MIP.

	CTRL		ABA		TBA	
	N_2	MIP	N_2	MIP	N_2	MIP
Total Pore Volume (cm^3/g)	0.09	0.27	0.13	0.18	0.11	0.19
Pore surface area (m^2/g)	35.53	82.39	68.53	47.85	43.62	44

threshold limit and was out of the reach of mercury. This is evident for ABA from the pore size distribution curve of N_2 adsorption in Fig. 9b. ABA has a higher volume of pores in the range 4.8–7 nm. Furthermore, it can be seen from Table 7 and the MIP pore size distribution curve (Fig. 9a), that there was a wide distribution of pore volume ranging from 3.8 to 16.1 nm for CTRL which was absent for the aluminosilicate modified samples. This is complementary to the N_2 adsorption results, CTRL has shown a wider range of pore volume (Table 7). The total pore volume and surface area calculated using the MIP mentioned in Table 8 are highest for the CTRL. This could be contributed by the pore range in model 1 (3.8–16.1 nm) that is absent for both TBA and ABA samples which showed a higher volume of mesopores in the range 4–9 nm. The behaviour of CTRL and TBA were comparable from both N_2 adsorption and MIP. However, the TBA showed an increase in total pore area and pore volume within the mesopore range 4.8–18 nm. In addition, the N_2 adsorption results of ABA-0E+ 0C - 3D showed a high volume of the lower end of mesopores range, around 2–9 nm in diameter (Fig. 9b).

3.2. Carbonation studies

3.2.1. Water loss and CO_2 uptake

Fig. 10 shows the water loss and subsequent CO_2 uptake during CO_2 curing for up to 24-hours. The water loss was calculated as the ratio of mass loss of water to the total initial water mass for each specimen [26]. In general, all the samples show a water loss of 25–30% at the end of 24 hours which is within the optimum water loss range for CO_2 uptake [26]. CTRL and TBA follow a similar trend in water loss (≈ 27%), whilst the water loss for ABA was slightly higher (≈30%). This could be because of excess free water formed as a by-product during the condensation of the ESA-APTES and Si-OH in the cement present on the surface. The CO_2 uptake of the CO_2 cured samples was calculated using the mass gain of samples during carbonation as follows [26,35]:

$$CO_2 uptake = \frac{M_{550} - M_{946}}{M_{cement}}$$

Where M_{550} and M_{946} were the masses of the samples at 550C and 946C, respectively, and Mcement was the mass of cement used. The mass loss between 550C and 946C was obtained by thermal analysis. The mass loss in this range corresponds to the carbon uptake during carbonation. After 24-hours of CO_2 curing, the CO_2 uptake of CTRL, ABA and TBA reached 9.0%, 9.6% and 8.7%, respectively, which was higher than that of the carbonated cement pastes in the literature [26]. TBA and CTRL had comparable levels of water loss and CO_2 uptake. In contrast, ABA showed increased levels of water loss and higher CO_2 uptake.

Fig. 11 shows the influence of CO_2 curing up to 24 hours on the hydration reaction of one-day-old cement pastes. The first two points in Fig. 11 represents the initial amount of hydration products (during in-mould curing and environmental chamber curing, respectively) before the samples underwent CO_2 curing. The carbonates mass is similar in both curing conditions for CTRL and TBA, representing the initial carbonate content in the CEM1. ABA showed a slight increase in carbonates before being cured in the carbonation chamber. This could have been because of the carbonation of the samples on manual handling. However, as both the in-mould and enivornmental chamber cured samples showed a similar increase in carbonates, it is more likely to have been due to the combination of amine and mesopores present in the sample, as previously identified in the literature [36]. In general, ABA showed

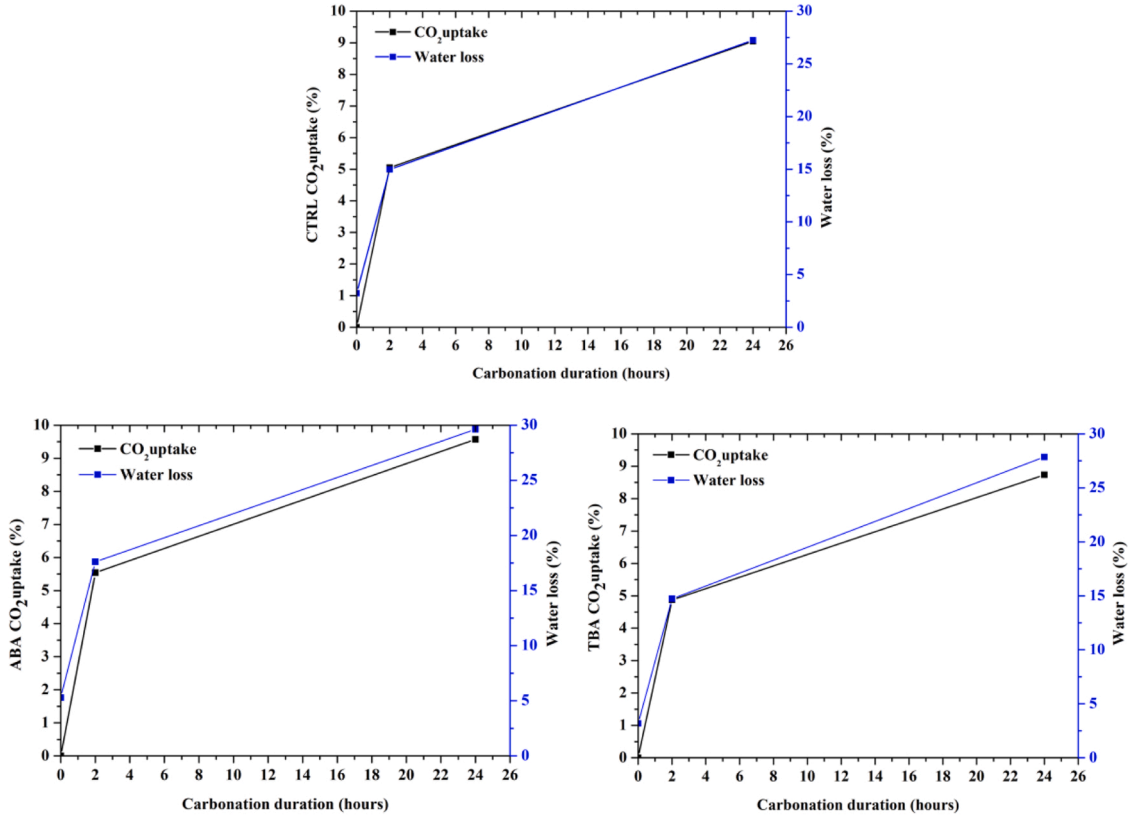

Fig. 10. CO_2 uptake and water loss after 2 h of enivornmental chamber curing; a. CTRL sample, b. ABA and c. TBA.

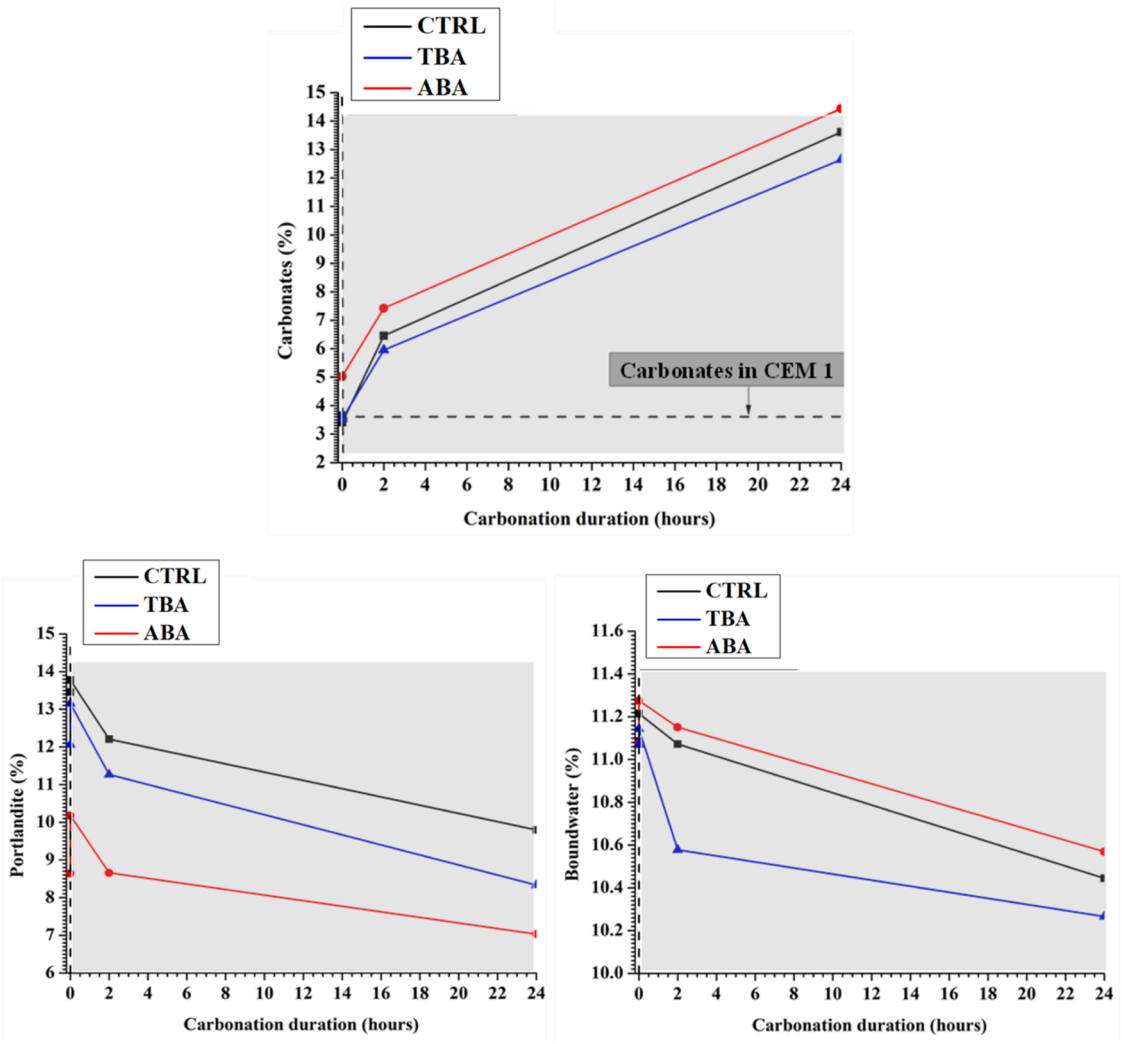

Fig. 11. Evaluation of carbonation on the content of carbonates, portlandite and bound water as measured by TGA during the 24-hour carbonation period.

higher carbonate formation, which is consistent with the higher CO_2 uptake (Fig. 9b.). Furthermore, the CO_2 uptake of the CTRL sample was slightly more than TBA which hence shows the increase in carbonates in Fig. 10. In addition, carbonation of TBA led to less portlandite than CTRL, which could have been because of pozzolanic reactivity of the silica rich ESA-TEOS. However, this is not the case, as the bound water produced is lower than CTRL. Hence, the lower portlandite content was because of the increased reactivity due to the combination of the C-S-H seeds formed on the 24-hour hydration (Section 4.1) and newly formed carbonate seeds that hindered the hydration of the unreacted clinker until further dissolution. This hypothesis would need further investigation under ageing, as is discussed later.

It is interesting to note that for ABA the portlandite at 2-hour CO_2 curing is comparable to the initially formed portlandite content (Fig. 11). This was not the case with CTRL and TBA. Furthermore, ABA's bound water content was the highest throughout the carbonation period. Together these findings indicate the high reactivity of ESA-APTES with Portland cement.

3.2.2. Phase identification

During the CO_2 curing, the change in hydration and carbonation products were monitored through XRD patterns. XRD spectra were acquired for all samples. The key can be referred to Table 6. Fig. 12 shows the XRD peaks of the 28-day carbonated samples. In general, it can be seen that on increasing CO_2 curing duration, the calcium carbonate peaks became more intense, especially around 29.3° and 35.9°, contrary to the portlandite peak, which reduced around 33.9°. The portlandite peak was missing for ABA at 63.8°, indicating lesser portlandite formed throughout the ageing process. In general, as the samples aged, the C_3S peak intensities at around 51.7° decreased. It is important to note that for ABA more calcium carbonate peaks were present when compared to TBA and CTRL. The Aft peak around 15.9° is absent for 3 days aged ABA sample irrespective of the CO_2 curing duration. This could be because of carbonation of Aft forming calcium carbonate and silica-alumina phases [26]. Portlandite peaks are more intense for the samples that were carbonated for a shorter duration than that for 24 hours for TBA.

3.2.3. TGA/DTG Analysis

Fig. 13 shows the amount of hydration products formed on ageing after subsequent CO_2 curing. CO_2 was diffused only up to 24 hours in the carbonation chamber hence the carbonates formed at 3, 7, and 28 days are due to the diffused CO_2 within the samples during the CO_2 curing. The shaded area represents the data obtained on ageing underwater, and the non-shaded area represents 2 hours of CO_2 curing (Fig. 13 a, c, e), and 24 hours of CO_2 curing (Fig. 13 b, d, f). In general, the carbonate content increased with age for the aluminosilicate modified samples compared to the carbonates formed on initial CO_2 diffusion for the 2 hours and 24 hour CO_2 cured samples. However, in the case of CTRL, on shorter CO_2 curing there was no significant increase in carbonates formed on ageing when compared to the initially formed carbonates.

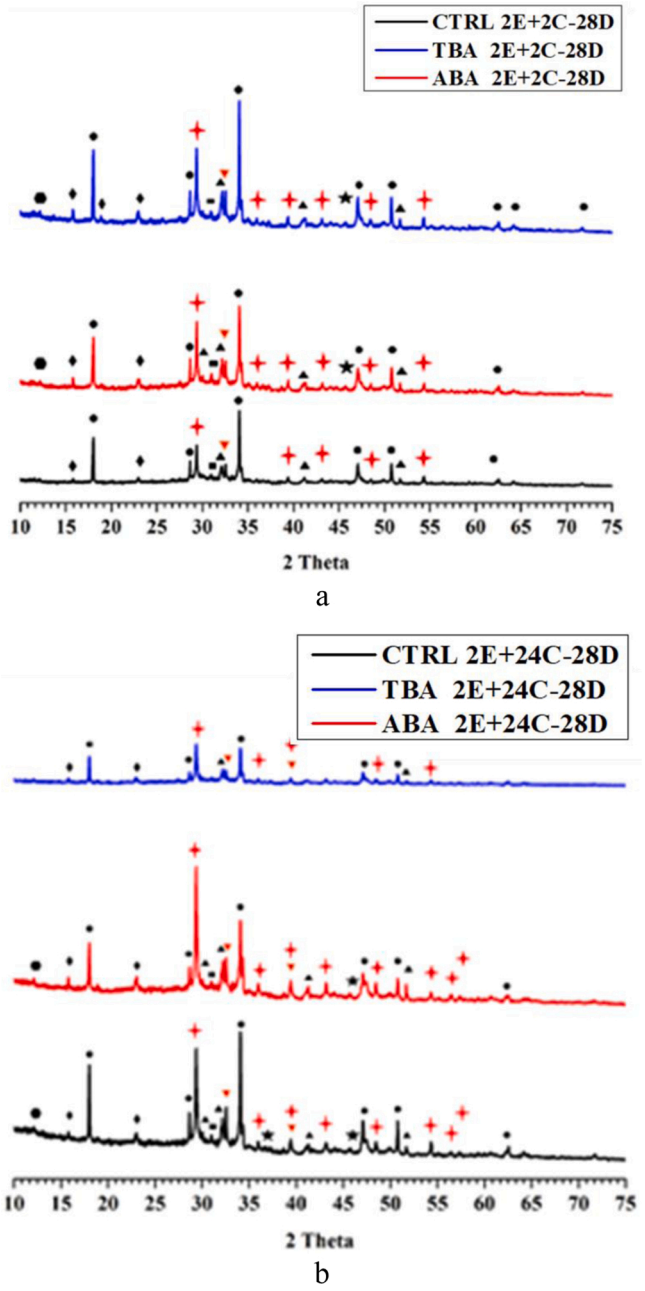

Fig. 12. Comparison of phases of 28-days aged samples that were initially environmental chamber cured for 2 hours followed by 2 hours and 24-hour carbonation curing.

Furthermore, on CO_2 curing, the carbonate content of the CTRL samples increased at 7 days, however, at the end of 28 days, the carbonate content reduced to the amount comparable to the content at the end 3 days (Fig. 13 b). This was because the carbonate content formed must have been unstable and hence decomposed. This instability of carbonates for CTRL is explained in Section 3.2.4. Both TBA and ABA showed different amounts of carbonates. In general, the carbonate content formed by ABA was higher than the TBA and CTRL, which confirms the XRD results. Unlike CTRL, the behaviour of the aluminosilicate modified samples at different ages after 2- and 24-hours CO_2 curing are different. For a 2-hour CO_2 curing period, the carbonates formed as the sample ages does not increase beyond 10% for the ABA. For TBA, the bound water had an inverse relation to the portlandite content as the sample ages. In the case of ABA, there was a decrease in carbonates as the sample aged.

Unlike 2-hours, for 24-hour CO_2 curing, the carbonates formed for ABA as the sample ages are higher when compared to CTRL and TBA. This could be due to high affinity of the amine groups for carbonate ions [36,37]. Furthermore, the rate of decrease of portlandite could be considered proportional to the rate of increase of bound water as the sample ages. This could imply possible pozzolanic reactions. In the case of TBA, on longer CO_2 curing (24 hours), the amount of carbonates decreased as the samples age when compared to the 2-hour CO_2 curing, this could be due to the instability of the carbonates formed during 7 days (Fig. 13). However, the rate of decrease of carbonates on ageing is low. Comparing the carbonate contents of TBA (Fig. 13 a and b), it can be seen that the samples have a limit of carbonate formation of ≈ 17%, irrespective of the duration of CO_2 curing (2-hours or 24-hours). The bound water and portlandite content formed indicates the increased reactivity of the C-S-H seeds combined with the nano carbonate seeds rather than pozzolanic reactivity. In Portland cement systems, higher calcium hydroxide content means higher carbonates as portlandite is more reactive than C_3S and C_2S [24]. However, this was not the case for TBA and ABA. Therefore, the hydration process did continue after carbonation. Furthermore, generally, carbonation causes starvation of water, leading to reduced hydration degree [24] however, this was not the case with addition of the ESA.

Furthermore, on CO_2 curing, the ABA's portlandite content decreased, and the bound water increased which could indicate that decalcification of C-S-H did not take place.

3.2.4. *Evaluation of carbonation of portlandite*

Table 9 gives the carbonation of portlandite within the cement matrix by comparing the amount of carbonates formed during the CO_2 curing and the total theoretical amount of carbonates that would have formed if the portlandite present in the non-carbonated samples underwent complete carbonation. The calculation was adapted from Rostami et al. [38]. For 3 day aged CTRL sample under 2 hours of CO_2 curing (CTRL-3D, 2E+2C), the amount of calcium carbonate that could be generated due to the carbonation of portlandite were calculated using the stochiometric Eq. 4. (100/74 x (12.75–12.32) %= 0.58%), where 100 and 74 are the molar masses of $CaCO_3$ and portlandite, respectively. By taking into account the initial amount of calcium carbonates in the non-carbonated 0E+ 0C (6.32%), the total calcium carbonates formed from only carbonation of portlandite should have been 6.90% (6.32%+ 0.58%) and this is very close to the amount formed (7.67%) meaning most of the carbonates were formed on decalcification of portlandite. The same was observed for early age TBA-2E+ 2C-3D. However, the calculated theoretical value was 8.96% $CaCO_3$ for TBA-2E+ 2C-28D. The actual amount of carbonates formed was 11.61% which indicates either carbonation of other phases such as calcium silicates and C-S-H or other mechanism theories of nucleation and seeding (Section 4.3). CTRL on ageing showed a similar trend to TBA. On increasing CO_2 curing duration (24 hours) of CTRL, the carbonates formed were more than the amount expected if assumed only portlandite carbonation. This indicates the possibilities of carbonation of other phases and can be confirmed using the mechanical strength test [39] (Fig. 18).

ABA samples at all ages of CO_2 curing showed more carbonates than the calculated theoretical amount of carbonates on complete carbonation of portlandite. The more carbonates observed could be due to the carbonation of anhydrous clinker. However, there needs further investigation to confirm the possible routes of formation of more carbonates.

3.2.5. *Pore structure characterisation*

The pore size distribution of samples subjected to 2 and 24-hour CO_2 curing is shown in Fig. 14 and Fig. 15. The variation in carbonation curing had a significant impact on the mesopore size distribution between 10 nm and 100 nm (MIP data). The relevance of the combined data from the nitrogen adsorption and the MIP is mentioned in Section 3.1.3. In general, from the MIP data in Fig. 14 and Fig. 15 a, c and e, it can be understood that the mesopore volume in the range between

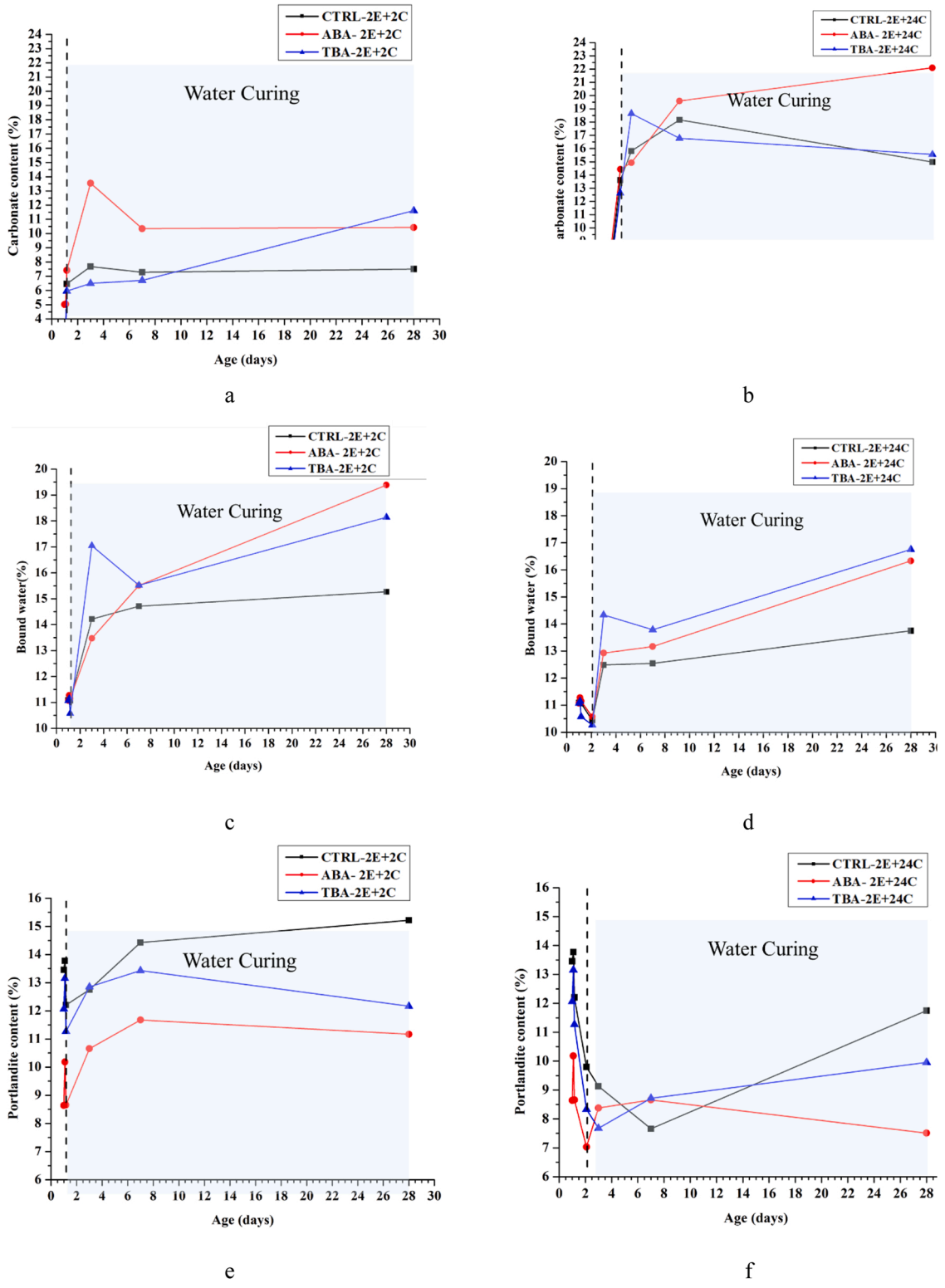

Fig. 13. Changes in carbonate content, bound water and portlandite content with age for 2-hour and 24-hour carbonation cured samples at.

10 nm and 100 nm has decreased on increasing the CO_2 curing time. A similar trend of CTRL and TBA is visible in the pore volume distribution in most cases except for the nitrogen adsorption-based pore volume distribution at 3 days age Fig. 14 b and Fig. 15 b). On increasing the CO_2 curing duration, the 7 day aged TBA (Fig. 15 c) showed higher pore volume around 51.05 nm when compared to CTRL, which shows the hydrate product filling the pores as mentioned in Section 3.1.3 [40]. However, the pore volume around 51.05 nm reduces on 28 days ageing, for TBA, indicating the availability of space for both hydration due to the formed nano carbonates and unhydrated clinker content. This is validated with the improvement in compressive strength (Fig. 16) and increase of bound water content and portlandite (Fig. 13 b and d.). The pore volume of ABA decreases on ageing around ≈ 36 nm for MIP for 2-hour carbonation duration (Fig. 16 a, c and e.). Furthermore, the

Table 9
Evaluation of the carbonation of portlandite by comparing the Actual amount and theoretical amount of calcium carbonate formed under curing protocol for CTRL, ABA and TBA.

Curing Protocol	Days	Specimen					
		CRTL		ABA		TBA	
		Ca $(OH)_2$	$CaCO_3$	Ca $(OH)_2$	$CaCO_3$	Ca $(OH)_2$	$CaCO_3$
0E+ 0C	3	12.32	6.32	13.44	4.36	15.1	3.21
	7	16.02	2.9	13.06	5.61	15.63	3.17
	28	18.72	2.9	14.53	3.66	16.6	2.97
2E+ 2C	3	12.75	7.67	10.66	13.55	12.85	6.5
	7	14.43	7.28	11.68	10.35	13.43	6.71
	28	15.22	7.5	11.17	10.43	12.17	11.61
2E+ 24C	3	9.13	15.82	8.38	14.93	7.68	18.64
	7	7.66	18.16	8.66	19.59	8.71	16.78
	28	11.75	14.98	7.51	22.1	9.95	15.56
Theoretical*	3	-	6.9	-	9.97	-	6.25
2E+ 2C	7		5.06		7.47		6.14
	28		7.63		8.2		8.96
Theoretical*	3	-	10.63	-	11.2	-	13.24
2E+ 24C	7		14.2		11.56		12.52
	28		12.31		13.14		11.95

* The theoretical amount of carbonates formed on the complete decomposition of the portlandite after 2-hour and 24-hours of CO_2 curing.

increase in porosity at ≈ 4–5 nm for the N_2 adsorption results (Fig. 16 f) reflects the small gel pores that further suggests the presence of additional C-S-H gel. Combining the N_2 adsorption and MIP results in Fig. 14 and Fig. 15, the ABA sample maintained a high pore volume around 4.8 nm irrespective of the curing protocols. The capillary pore size between 10 nm and 50 nm was the most affected region in the case of ABA under the various curing conditions. This indicates that the carbonation and subsequent hydration did not affect the C-S-H gel pores. This finding is in good corroboration with the unaffected mechanical performance.

3.2.6. Compressive strength result

Fig. 16 shows the compressive strength results of the 28 days aged mortar samples. The addition of ESAs led to a reduction in the strength of non-carbonated samples and samples carbonated for a shorter duration. Indeed, with 2 hours CO_2 curing the results were almost identical to 0E+ 0C even though the deviation of results were significant, showing that such a short period of CO_2 curing has little effect. Comparatively significant difference came with longer CO_2 curing duration. On 24-hour CO_2 curing, the CTRL loses strength, but the TBA increases. Although the ABA carbonates more, it would not affect its mechanical performance. This could further indicate decalcification did not take place as discussed in Section 3.2.4. ABA seems to be unaffected by curing regime and gives the same strength regardless. This could be further valididated with the controllability aspect of sol-gel technology [41]. Whereas for the CTRL this is clearly the case.

CTRL and TBA show the same amount of CO_2 loss (Fig. 10). However, TBA has a higher compressive strength on increasing the CO_2 curing, from which it could be suggested that the carbonation on CTRL is decalcifying the C-S-H gel, hence more carbonates than that the amount formed on complete carbonation of portlandite (refer to Section 3.2.4) are formed. This is not the case for TBA, as it gets stronger. Suggesting that the ESA-TEOS in TBA is donating Si to form C-S-H or even donating Al to form C-A-S-H (refer Fig. 4). Furthermore, the improvement in strength of TBA-2E+ 24C could be due to the combined effect of formation of dense carbonates and hydration products.

4. Discussion

4.1. Hydration

The effects on the hydration of the cement were different depending on the different use of sol-gel precursors TEOS or APTES.

The use of APTES, as in ABA, led to a longer dormant period followed by a sharp, intensive period of rapid hydration. The retarding effect of the APTES was most likely due to the dispersive nature of the -NH_2 species [32,42] a steric impediment, that slowed down the C_3S dissolution. This was indicated in this work by a decrease in portlandite formation at 24 hours (Fig. 7). Despite the extended dormant period, measurements of bound water and portlandite at three days, suggest that the use of APTES increased the formation of hydration products. These findings can be explained by the dispersive characteristics of APTES upon the Portland cement particles, due to the hydrophilic amino-alkyl chain (H_2N-$(CH_2)3Si(OC_2H_5)_3$) that providing steric repulsion [43]. TBA showed a similar trend to CTRL.

4.2. Carbonation

For the CTRL samples, the volume of carbonates formed after 2E+ 2C curing was similar to that formed after 0E+ 0C and 2E+ 0C curing. This suggests that two hours of CO_2 curing was insufficient for the absorption of CO_2 for longer term carbonation to occur. For 24 hours of CO_2 curing (2E+24C) there was a clear increase in carbonates at 3 days suggesting that CO_2 did react with hydration products to form calcium carbonate. However, the volume of carbonates present in the samples after 3 days was largely the same at 28 days. This suggests that there was no longer-term storage of CO_2 in the samples, and no additional carbonation beyond that which occurred principally within the chamber.

The carbonation behaviour of the aluminosilicate-modified samples was dependent on the functionality of the aluminosilicate. In contrast, for ABA there was an increase in carbonate content as they aged – i.e. after they were removed from the chamber. This indicates that CO_2 was bound within the paste for later use. Furthermore, for ABA the use of just two hours CO_2 curing (2E+2C) led to higher carbonate contents than the CTRL, although clearly 24 hours of CO_2 curing led to greater carbonates both initially and in the longer-term.

The results from TBA in terms of carbonation were less conclusive than for ABA. Whilst higher carbonate contents were measured than in the CTRL the general pattern was similar to that of the CTRL suggesting perhaps minimal binding of CO_2.

Interestingly the increased formation of carbonates did not necessarily lead to an improvement in compressive strength. Indeed, for the CTRL the formation of carbonates led to a loss in mechanical strength. On the other hand, ABA was largely unaffected; whilst TBA did increase. Because water loss increases during CO_2 curing it was considered that differences in how the water may be held within the hydration products may be responsible for the differences observed. The relationship between water loss during CO_2 curing and the 28 days compressive strength is shown in Fig. 17, whilst Fig. 18 compares the carbonate content with bound water content. It is well known that water loss can be detrimental to the long-term hydration of a cement paste. For the CTRL the high-water loss may have led to water starvation, which in turn hindered hydration and hence the decrease in the bound water and mechanical performance of the sample. This would be consistent with observations that the shorter curing carbonation, which primarily only affected CH, led to less loss in strength than the longer carbonation curing period were there was also decalcification of C-S-H. Whilst ABA and TBA had similar water losses (Fig. 17) to the CTRL the remaining bound water content was in all cases higher than the CTRL (Fig. 18). There is some indication that for these pastes there was less decalcification of C-S-H on carbonation. However, a complete understanding of this aspect is beyond the scope of the paper.

On closer observation, comparing Table 10 and Fig. 18, the % volume of nanopores < 10 nm (indicative of C-S-H gel) and the increase of bound water indicates that the increase in carbonates was not because of decalcification of the C-S-H as the mechanical performance of the 28 days samples did not decrease on carbonation. Thus, it can be suggested that there was a controlled carbonation in the case of ABA due to the

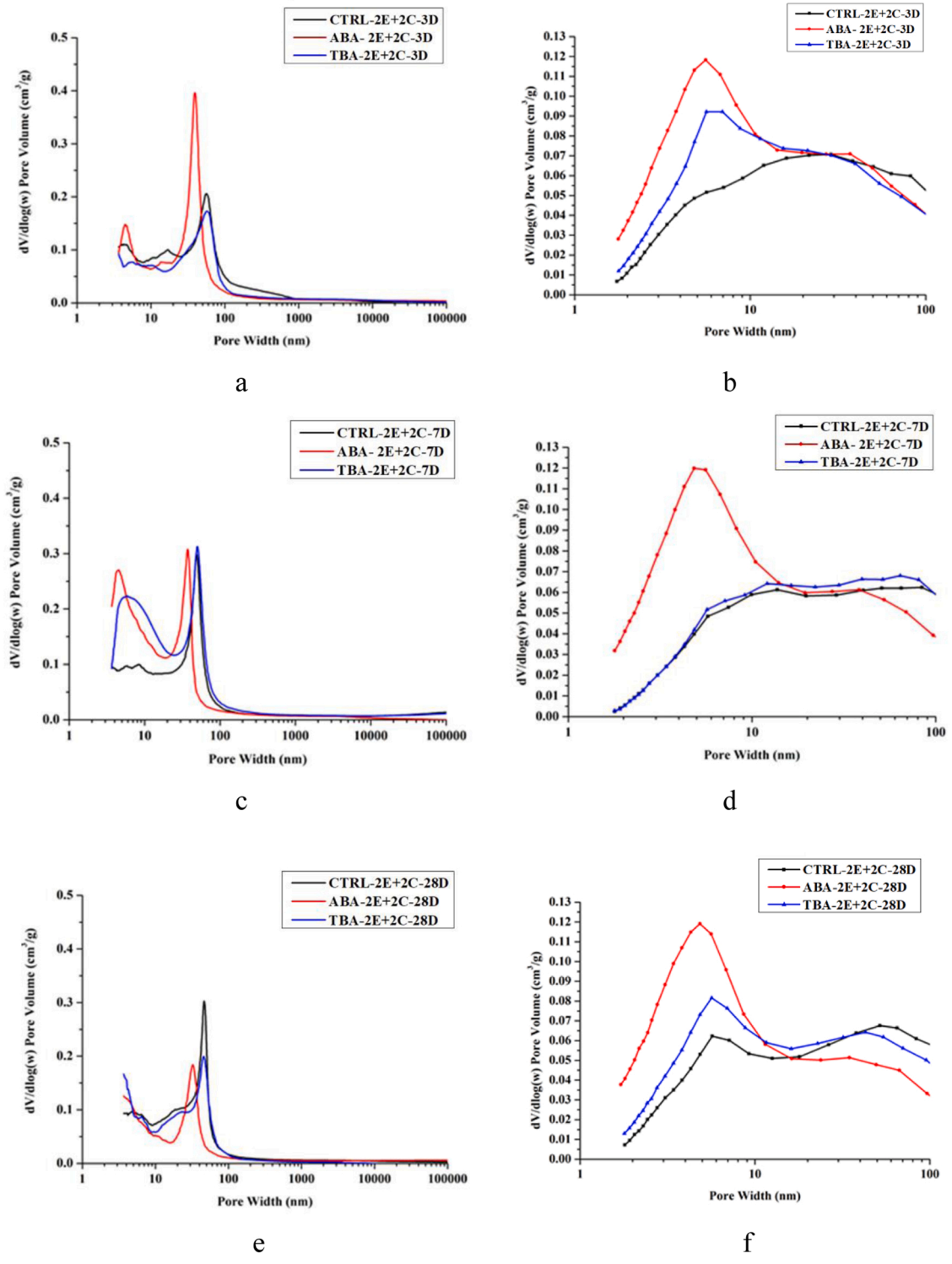

Fig. 14. Pore volume distribution of samples under curing regime 2E+ 2C; MIP data a, c and e; Nitrogen adsorption data b, d and f.

homogenously dispersed medium.

At 28 days age, TBA showed high mechanical performance (Fig. 16). Comparing the results in Fig. 18 with the Table 10, the carbonates formed enhanced the pozzolanic and nucleation reaction, which improved the mechanical performance [18,44,45].

4.3. Mechanism of CO_2 interaction within the cement matrix

Fig. 19 shows schematically the postulated reaction mechanisms based on the research finding indications and literature when CO_2 is diffused in a 24-hour hydrated cement matrix. In the case of CTRL samples when CO_2 diffuses into the 24 hours hydrated samples, initially carbonates were formed as shown in stage b (Fig. 19). However, as the carbonation progressed, it caused decalcification of portlandite and C-S-H. Furthermore, in general, at all stages a, b and c (Fig. 19), there was a delay in the progress of hydration due to the water lost during CO_2 uptake, promoting water starvation in the system.

For TBA, as the CO_2 diffused into the 24 hour hydrated samples, the

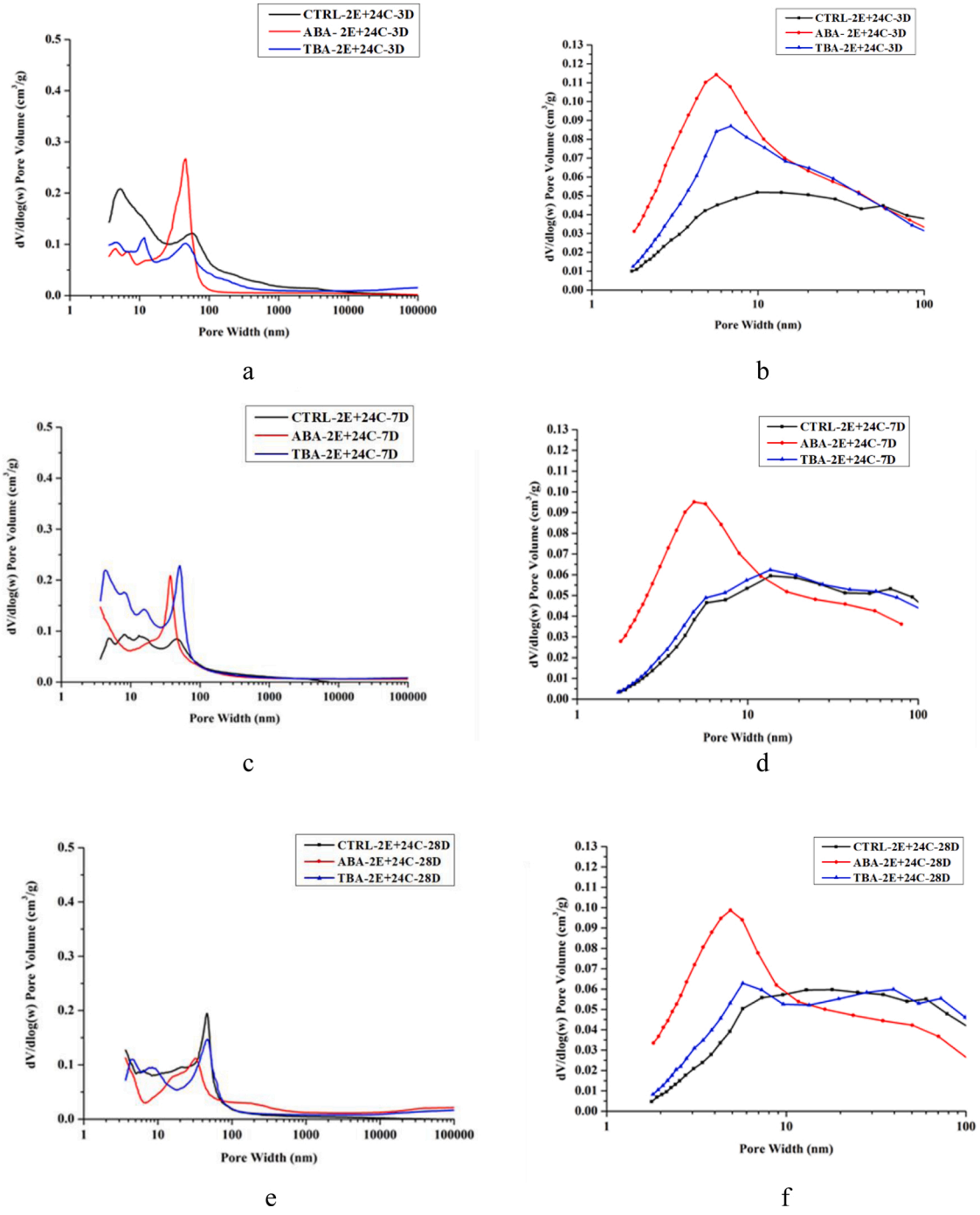

Fig. 15. Pore volume distribution of samples under the curing regime 2E+ 24C; MIP data a, c and e; Nitrogen adsorption data b, d and f.

carbonates formed could be attributed to the carbonation of unhydrated clinker (stage b in Fig. 19.). However, as the reactions proceeded, it could be seen that the portlandite content decreased and bound water and carbonates increased (stage c in Fig. 19. and Fig. 13). The bound water content increased as ESA-TEOS had pozzolanic nature, and carbonates formed behaved as seeding sites. Hence there was a reduction in carbonates on progress of hydration reactions. Thus, the carbonates formed enhanced the pozzolanic and nucleation reactions, which improved the mechanical performance [18,45].

ABA indicates an interesting reaction mechanism when amine functionalised aluminosilicates replaced 1% by mass of the cement. The amine presents in ABA, even before CO_2 curing showed higher adsorption of atmospheric CO_2 (carbonate seen in stage a in Fig. 19.). This was due to their high affinity towards atmospheric CO_2. Stage b (Fig. 19). shows the hydrolysis and condensation of ESA-APTES leaving the unhydrolysed amine. The alumina-silica network within the cement matrix had non-hydrolysed amine groups that created a well dispersed medium for controlled reaction mechanisms. Hence, for ABA samples, the enhanced carbonate formation could be due to the combined effect of the chemical bonding between the unhydrolysed amine species and CO_2, which on the exothermic hydration reaction, created sufficient energy to break the chemical bonds and release the carbonate ions [46]. These ions reacted with the Ca^{2+} ions in the medium to form carbonates. There was a very stable performance for ABA even though a high carbonate content was formed. This could be because there was always a competition between carbonation and hydration and enough water

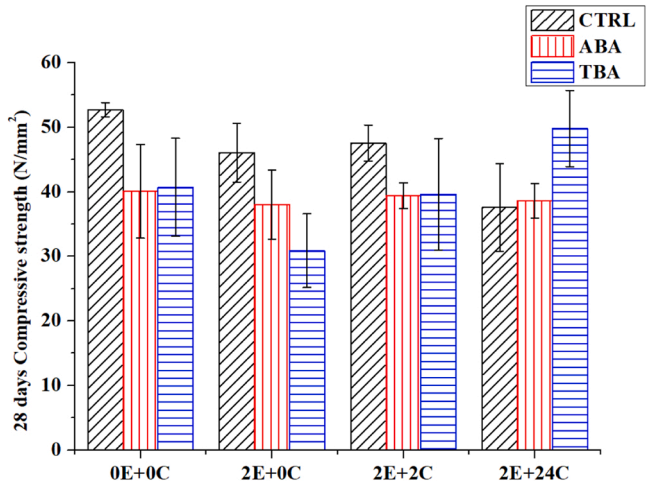

Fig. 16. Compressive strength results of the 28 days aged samples under different curing conditions.

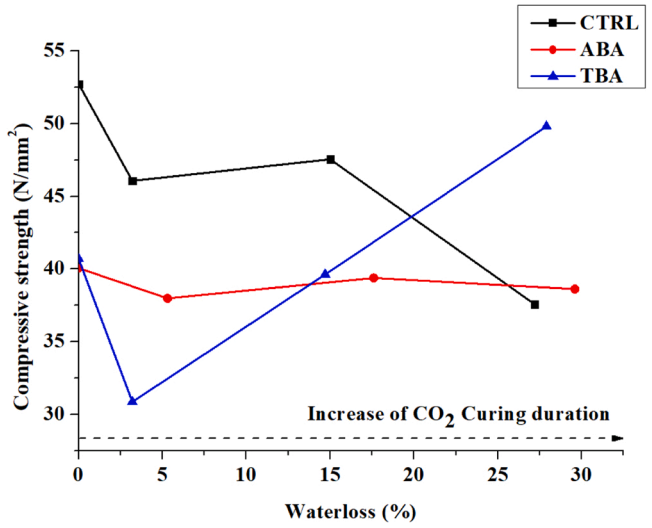

Fig. 17. Evaluation of mechanical performance of samples on increase of water loss.

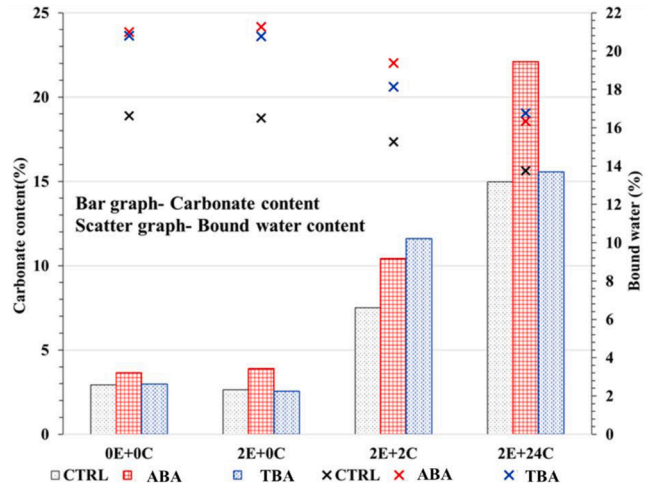

Fig. 18. Comparison bound water content and carbonate content of 28 days aged samples.

Table 10
Comparison of carbonates formed on ageing to the initially formed carbonates on carbonation curing.

Curing Protocol	2 C			24 C		
	CTRL	ABA	TBA	CTRL	ABA	TBA
Initially formed*	6.4	7.42	5.96	13.6	14.44	12.65
3 Days aged	7.67	13.55	6.5	15.82	14.93	18.65
7 Days aged	7.28	10.35	6.71	18.16	19.59	16.78
28 Days aged	7.5	10.43	11.61	14.98	22.1	15.56

* The initially formed carbonate content is the amount of carbonates in the sample present immediately after carbonation curing in the carbonation chamber

availability. Also, the well dispersed matrix prevented the formation of any barrier layer, indicating some level of controllability. Such a uniformly dispersed medium always maintained a certain level of reaction, whether carbonation or hydration, could have enabled a consistent performance to some degree considering the variability in the results [29].

5. Conclusions

The controllability of the carbonation reaction on addition of ESA-TEOS and ESA-APTES was investigated in this paper. The results indicate that there is a possibility to tailor the carbonation by addition of functionalised additions that can target specific modes of reactions (either nucleation or chemical adsorption). Such a system could provide a more stability to the overall performance of the carbonated cement matrix than when cement paste alone is carbonated. A key feature of controlling carbonation using ESAs was that there was a further reduction in the use of cement (in this case 1% replacement by weight). The main conclusions drawn from the paper were:

1. For all samples the water loss increased on increase of CO_2 curing time. However, only for the CTRL carbonated samples, water starvation and subsequent hindrance of hydration was observed.
2. The indicated increased reactivity and pozzolanic behaviour of TBA and ABA has been identified during the hydration studies.
3. Addition of ESA-APTES could show a more homogeneously dispersed medium.
4. Addition of small quantities of such ESA nanoparticles increases the reactivity of unhydrated clinker and prevent decalcification of hydration products.
5. There was a possible alteration of the carbonation and subsequent hydration mechanism.
6. It was determined that 1% of addition of the ESA showed improvement in the carbonate formation compared to the control samples without the aluminosilicates.
7. The carbonation efficiency was the highest for ABA. In addition, the amine groups hanging in the aluminosilicates adsorbed ≈ 2% of atmospheric CO_2 due to the high affinity of amine and CO_2.
8. TBA carbonation and subsequent hydration were enhanced possibly by nucleation and seeding effect of the nano-carbonates formed on carbonation curing combined with pozzolanic reactions that led to a decrease in portlandite.
9. ABA had enhanced carbonation and subsequent hydration, possibly due to the ESA creating a uniformly dispersed solution that prevented the formation of a passivation layer. This indicated that there could have been continuous carbonation or hydration reactions occurring.

CRediT authorship contribution statement

Pooja Anil Kumar Nair: Conceptualization, Writing – original draft. **Juliana Calabria-Holley**: Writing – review & editing, Visualization,

Table 11
Evaluation of the microstructure of the 28 days aged sample comparing the bound water and carbonate content.

	CTRL			ABA			TBA		
	Pore Volume < 10 nm	Bound water content	Calcium carbonate content	Pore Volume < 10 nm	Bound water content	Calcium carbonate content	Pore Volume < 10 nm	Bound water content	Calcium carbonate content
	(%)	(%)	(%)	(%)	(%)	(%)	(%)	(%)	(%)
0E+ 0 C	7.55	16.62	2.94	13.85	20.99	3.66	9.59	20.81	2.97
2E+ 0 C	6.1	16.51	2.63	13.99	21.26	3.88	8.6	20.77	2.55
2E+ 2 C	7.2	15.27	7.5	13.83	19.39	10.43	8	18.14	11.61
2E+ 24 C	7.7	13.75	14.98	16.46	16.33	22.1	7.25	16.75	15.56

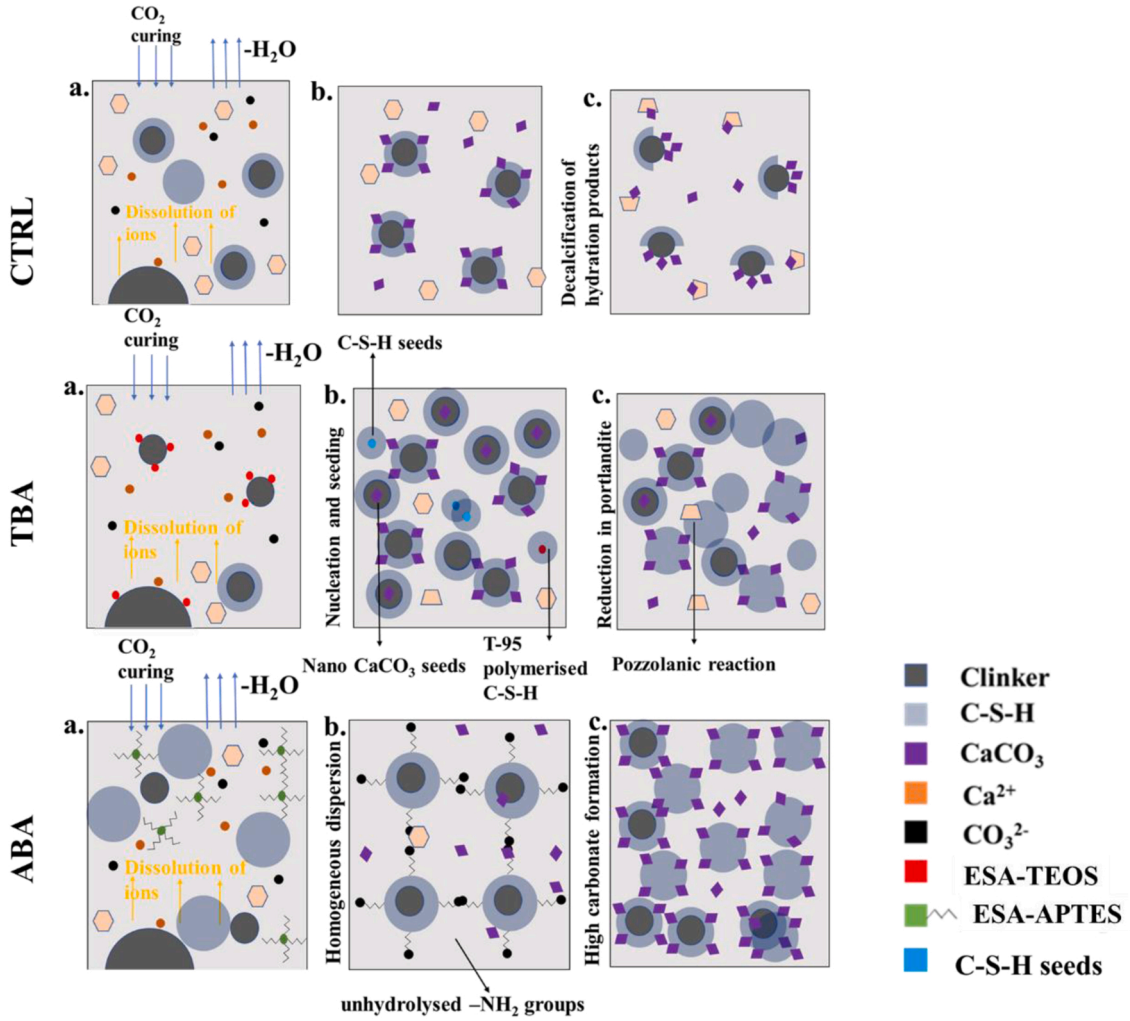

Fig. 19. The reaction mechanisms due to the diffused CO_2 within the 24 hour hydrated cement matrix with and without ESA.

Supervision. **Kevin Paine**: Writing – review & editing, Visualization, Supervision.

Declaration of Competing Interest

The authors declare that they have no known competing financial interests or personal relationships that could have appeared to influence the work reported in this paper.

Data Availability

Data will be made available on request.

Acknowledgements

The authors acknowledge Olivier Camus, William Bazeley and Martin Naidu, technicians within the Architecture and Civil Engineering Laboratory at the University of Bath, for their support with the experimental work.

References

[1] A. Hasanbeigi, L. Price, H. Lu, W. Lan, Analysis of energy-efficiency opportunities for the cement industry in Shandong Province, China: a case study of 16 cement plants, Energy 35 (2010) 3461–3473, https://doi.org/10.1016/j.energy.2010.04.046.

[2] A. Naqi, J.G. Jang, Recent progress in green cement technology utilizing low-carbon emission fuels and raw materials: a review, Sustain 11 (2019), https://doi.org/10.3390/su11020537.

[3] G. Habert, S.A. Miller, V.M. John, J.L. Provis, A. Favier, A. Horvath, K.L. Scrivener, Environmental impacts and decarbonization strategies in the cement and concrete industries, Nat. Rev. Earth Environ. 1 (2020) 559–573, https://doi.org/10.1038/s43017-020-0093-3.

[4] S. Monkman, P.A. Kenward, G. Dipple, M. MacDonald, M. Raudsepp, Activation of cement hydration with carbon dioxide, J. Sustain. Cem. Mater. 7 (2018) 160–181, https://doi.org/10.1080/21650373.2018.1443854.

[5] M. Jarraud, A. Steiner, Climate Change, Synth. Report. (2014) 2012, https://doi.org/10.1017/CBO9781139177245.003.

[6] H. Naseri, H. Jahanbakhsh, P. Hosseini, F. Moghadas Nejad, Designing sustainable concrete mixture by developing a new machine learning technique, J. Clean. Prod. 258 (2020), 120578, https://doi.org/10.1016/j.jclepro.2020.120578.

[7] S. Monkman, M. MacDonald, R.D. Hooton, P. Sandberg, Properties and durability of concrete produced using CO_2 as an accelerating admixture, Cem. Concr. Compos. 74 (2016) 218–224, https://doi.org/10.1016/j.cemconcomp.2016.10.007.

[8] N. Al-ayish, Environmental Impact of Concrete Structures – with Focus on Durability and Resource Efficiency, 2017.

[9] M. Rubenstein, Emissions from the Cement Industry, State Planet Earth Institute/Colombia Univ. (2012). https://blogs.ei.columbia.edu/2012/05/09/emissions-from-the-cement-industry/.

[10] K. Scrivener, F. Martirena, S. Bishnoi, S. Maity, Calcined clay limestone cements (LC3), Cem. Concr. Res. 114 (2018) 49–56, https://doi.org/10.1016/j.cemconres.2017.08.017.

[11] A. Joshaghani, The effects of zeolite as supplementary cement material on pervious concrete, International Concrete Sustainability Conference Washington D.C.At: Washington DC, United States (2016).

[12] P. Suraneni, J. Weiss, Examining the pozzolanicity of supplementary cementitious materials using isothermal calorimetry and thermogravimetric analysis, Cem. Concr. Compos. 83 (2017) 273–278, https://doi.org/10.1016/j.cemconcomp.2017.07.009.

[13] E. Gartner, T. Sui, Alternative cement clinkers, Cem. Concr. Res. 114 (2018) 27–39, https://doi.org/10.1016/j.cemconres.2017.02.002.

[14] A. Naceri, M.C. Hamina, Use of waste brick as a partial replacement of cement in mortar, Waste Manag 29 (2009) 2378–2384, https://doi.org/10.1016/j.wasman.2009.03.026.

[15] A. Usman, M.B. Ibrahim, N. Bala, Effect of amorphous silica ash used as a partial replacement for cement on the compressive and flexural strengths cement mortar, IOP Conf. Ser. Earth Environ. Sci. 140 (2018), https://doi.org/10.1088/1755-1315/140/1/012124.

[16] S.A. Mangi, N. Jamaluddin, M.H. Wan Ibrahim, A.H. Abdullah, A.S.M. Abdul Awal, S. Sohu, N. Ali, Utilization of sugarcane bagasse ash in concrete as partial replacement of cement, IOP Conf. Ser. Mater. Sci. Eng. 271 (2017), https://doi.org/10.1088/1757-899X/271/1/012001.

[17] B.J. Zhan, D.X. Xuan, C.S. Poon, C.J. Shi, S.C. Kou, Characterization of C–S–H formed in coupled CO_2–water cured Portland cement pastes, Mater. Struct. Constr. 51 (2018), https://doi.org/10.1617/s11527-018-1211-2.

[18] S. Monkman, B.E.J. Lee, K. Grandfield, M. MacDonald, L. Raki, The impacts of in-situ carbonate seeding on the early hydration of tricalcium silicate, Cem. Concr. Res. 136 (2020), 106179, https://doi.org/10.1016/j.cemconres.2020.106179.

[19] H. El-Hassan, Y. Shao, Carbon storage through concrete block carbonation, J. Clean. Energy Technol. 2 (2013) 287–291, https://doi.org/10.7763/jocet.2014.v2.141.

[20] D. Zhang, Z. Ghouleh, Y. Shao, Review on carbonation curing of cement-based materials, J. CO_2 Util. 21 (2017) 119–131, https://doi.org/10.1016/j.jcou.2017.07.003.

[21] X. Li, T.C. Ling, Instant CO_2 curing for dry-mix pressed cement pastes: Consideration of CO_2 concentrations coupled with further water curing, J. CO_2 Util. 38 (2020) 348–354, https://doi.org/10.1016/j.jcou.2020.02.012.

[22] Y. Chun, T.R. Naik, R.N. Kraus, Carbon dioxide sequestration in concrete in different curing environments, Proc. Coventry Univ. Int. Conf. Sustain. Constr. Mater. Technol. Coventry. (2007) 18–24.

[23] T. Chen, X. Gao, Use of carbonation curing to improve mechanical strength and durability of pervious concrete, ACS Sustain. Chem. Eng. 8 (2020) 3872–3884, https://doi.org/10.1021/acssuschemeng.9b07348.

[24] Z. He, Z. Li, Y. Shao, Effect of carbonation mixing on CO_2 uptake and strength gain in concrete, J. Mater. Civ. Eng. 29 (2017) 04017176, https://doi.org/10.1061/(asce)mt.1943-5533.0002031.

[25] P. Liu, Y. Chen, Z. Yu, R. Zhang, Effect of temperature on concrete carbonation performance, Adv. Mater. Sci. Eng. 2019 (2019) 1–7, https://doi.org/10.1155/2019/9204570.

[26] T. Chen, X. Gao, Effect of carbonation curing regime on strength and microstructure of Portland cement paste, J. CO_2 Util. 34 (2019) 74–86, https://doi.org/10.1016/j.jcou.2019.05.034.

[27] S.J. Gerdemann, W.K. O'Connor, D.C. Dahlin, L.R. Penner, H. Rush, Ex situ aqueous mineral carbonation, Environ. Sci. Technol. 41 (2007) 2587–2593, https://doi.org/10.1021/es0619253.

[28] W. Ding, L. Fu, J. Ouyang, H. Yang, CO_2 mineral sequestration by wollastonite carbonation, Phys. Chem. Miner. 41 (2014) 489–496, https://doi.org/10.1007/s00269-014-0659-z.

[29] A. Santos, J.A. Toledo-Fernández, R. Mendoza-Serna, L. Gago-Duport, N. De La Rosa-Fox, M. Piñero, L. Esquivias, Chemically active silica aerogel - Wollastonite composites for CO 2 fixation by carbonation reactions, Ind. Eng. Chem. Res. 46 (2007) 103–107.

[30] V. Morales-Flórez, L. Esquivias, A. Santos, Sol-Gel Materials for Carbon Mineral Sequestration, in: Sol-Gel Process. Conv. Altern. Energy, 2012: pp. 177–199. https://doi.org/10.1007/978–1-4614–1957-0.

[31] P.A.K. Nair, K. Paine, J. Calabria-Holley, CO_2 Capture Adsorbents using Sol-gel Technology to develop a Carbon Neutral Cement, in: B. Abstr (Ed.), Int. Sol-Gel Conf, 2019, p. 312.

[32] X.M. Kong, H. Liu, Z.B. Lu, D.M. Wang, The influence of silanes on hydration and strength development of cementitious systems, Cem. Concr. Res. 67 (2015) 168–178, https://doi.org/10.1016/j.cemconres.2014.10.008.

[33] J. Calabria-Holley, K. Paine, S. Papatzani, Effects of nanosilica on the calcium silicate hydrates in Portland cement–fly ash systems, Adv. Cem. Res. 27 (2014) 187–200, https://doi.org/10.1680/adcr.13.00098.

[34] F. Švegl, J. Šuput-Strupi, L. Škrlep, K. Kalcher, The influence of aminosilanes on macroscopic properties of cement paste, Cem. Concr. Res. 38 (2008) 945–954, https://doi.org/10.1016/j.cemconres.2008.02.006.

[35] J.G. Jang, H.K. Lee, Microstructural densification and CO_2 uptake promoted by the carbonation curing of belite-rich Portland cement, Cem. Concr. Res. 82 (2016) 50–57, https://doi.org/10.1016/j.cemconres.2016.01.001.

[36] A. Wagner, B. Steen, G. Johansson, E. Zanghellini, P. Jacobsson, P. Johansson, Carbon dioxide capture from ambient air using amine-grafted mesoporous adsorbents, Int. J. Spectrosc. 2013 (2013) 1–8, https://doi.org/10.1155/2013/690186.

[37] J. Van Straelen, F. Geuzebroek, The thermodynamic minimum regeneration energy required for post-combustion CO_2 capture, Energy Procedia 4 (2011) 1500–1507, https://doi.org/10.1016/j.egypro.2011.02.017.

[38] V. Rostami, Y. Shao, A.J. Boyd, Z. He, Microstructure of cement paste subject to early carbonation curing, Cem. Concr. Res. 42 (2012) 186–193, https://doi.org/10.1016/j.cemconres.2011.09.010.

[39] C.A. Fioroni, M.D. de, M. Innocentini, G.M. de Los Dolores, G.H.D. Tonoli, G.R. de Paula, H. Savastano, Cement-based corrugated sheets reinforced with polypropylene fibres subjected to a high-performance curing method, Constr. Build. Mater. 262 (2020), 120791, https://doi.org/10.1016/j.conbuildmat.2020.120791.

[40] Q. Zeng, K. Li, T. Fen-Chong, P. Dangla, Pore structure of cement pastes through NAD and MIP analysis, Adv. Cem. Res. 28 (2016) 23–32, https://doi.org/10.1680/adcr.14.00109.

[41] P.A.K. Nair, W.L. Vasconcelos, K. Paine, J. Calabria-Holley, A review on applications of sol-gel science in cement, Constr. Build. Mater. 291 (2021), 123065, https://doi.org/10.1016/j.conbuildmat.2021.123065.

[42] R. Guttmann, A.F. Sax, Dispersion interactions and the stability of amine dimers, ChemistryOpen 6 (2017) 571–584, https://doi.org/10.1002/open.201700052.

[43] G. Land, D. Stephan, The influence of nano-silica on the hydration of ordinary Portland cement, J. Mater. Sci. 47 (2012) 1011–1017, https://doi.org/10.1007/s10853-011-5881-1.

[44] Tailored Calcium-Silicate-Hydrates: a sol-gel approach to nucleation seedingShakil, M. (Author). 16 Sep 2020.

[45] Z. Tu, C. Shi, N. Farzadnia, Effect of limestone powder content on the early-age properties of CO_2-cured concrete, J. Mater. Civ. Eng. 30 (2018) 04018164, https://doi.org/10.1061/(asce)mt.1943-5533.0002232.

[46] W. Xie, H. Li, M. Yang, L. He, H. Li, Green chemical engineering CO 2 capture and utilization with solid waste, Green. Chem. Eng. ((2022), https://doi.org/10.1016/j.gce.2022.01.002.